CHALMERS

Evaluation of the arch crown connection of the New Svinesund Bridge

Finite element modelling of the long-term structural response

Master's Thesis in the Master's programme Structural Engineering and Building Performance Design

PER LINDBERG
JONAS NILSSON

Department of Civil and Environmental Engineering
Division of Structural Engineering
Concrete Structures
CHALMERS UNIVERSITY OF TECHNOLOGY
Göteborg, Sweden 2010
Master's Thesis 2010:50

MASTER'S THESIS 2010:50

Evaluation of the arch crown connection of the New Svinesund Bridge

Finite element modelling of the long-term structural response

Master's Thesis in the *Master's programme Structural Engineering and Building Performance Design*

PER LINDBERG

JONAS NILSSON

Department of Civil and Environmental Engineering
Division of Structural Engineering
Concrete Structures
CHALMERS UNIVERSITY OF TECHNOLOGY
Göteborg, Sweden 2010

Evaluation of the arch crown connection of the New Svinesund Bridge
Finite element modelling of the long-term structural response

Master's Thesis in the *Master's programme Structural Engineering and Building Performance Design*
PER LINDBERG
JONAS NILSSON

Examensarbete 2010:50
Department of Civil and Environmental Engineering
Division of Structural Engineering
Concrete Structures
Chalmers University of Technology
SE-412 96 Göteborg
Sweden
Telephone: + 46 (0)31-772 1000

Cover: The New Svinesund Bridge, Vägverket(2007)

Chalmers Reproservice
Göteborg, Sweden 2010

Evaluation of the arch crown connection of the New Svinesund Bridge
Finite element modelling of the long-term structural response

Master's Thesis in the *Master's programme Structural Engineering and Building Performance Design*

PER LINDBERG
JONAS NILSSON
Department of Civil and Environmental Engineering
Division of Structural Engineering
Concrete Structures
Chalmers University of Technology

ABSTRACT

The New Svinesund Bridge was opened for traffic in 2005 in connection with the 100 year dissolution of the union between Sweden and Norway. The new bridge connects Sweden and Norway over the Ide fjord at Svinesund and forms an important link in the European highway system. For one of the more essential parts of the bridge, the arch crown connection, the construction process was changed compared to the original plan. Before the crown segment was cast, steel bars were inserted between the arch halves. The forces in the tendons stabilizing the arch halves were then adjusted and the steel bars were loaded. It has since then been uncertain if this deviation in constructing the arch would lead to problems in the future due to long-term effects.

A finite element (FE) model of the New Svinesund Bridge was developed by Plos and Movaffaghi (2004) including a simplified analysis of the construction of the bridge. This model has further been developed by Canovic and Goncalves (2005), and includes the sequential construction of the arch, with a material model describing creep and temperature dependency.

The aim of this Master's thesis was to further develop the already existing FE-model, and to perform an improved analysis of the arch crown connection taking long-term effects into account. The model in this Master's thesis has been updated with a more accurate launching procedure, material properties to account for creep and shrinkage, and an analysis describing the entire service life of the bridge. From the sectional forces obtained from the analysis, a more detailed study of the arch crown connection was performed.

It was found that the influence of creep and shrinkage has an unfavorable effect on the sectional response of the arch crown in the long time perspective. Even if the long-term effects have a negative influence on the arch crown, the critical events was found to occur during the construction of the arch. Concerning the steel bars it was found that they will carry an increasing part of the normal force over time due to the long-term effects.

After a detailed study of the sectional response and of the areas where the steel bars are attached, it was found that the state of stresses would not cause any problems regarding the future performance of the arch crown.

Key words: Svinesund, Bridge, Arch, Finite element, Long-term effects, Shrinkage, Creep

Utvärdering av verkningssätt och kraftfördelning i bågens hjässa i nya Svinesundsbron

Examensarbete inom Masterprogrammet Structural Engineering and Building Performance Design

PER LINDBERG
JONAS NILSSON
Institutionen för Bygg- och miljöteknik
Avdelningen för Konstruktionsteknik
Betongbyggnad
Chalmers tekniska högskola

SAMMANFATTNING

Den nya Svinesundsbron öppnades för trafik år 2005 i samband med 100-årsjubileet av unionsupplösningen mellan Sverige och Norge. Den nya bron förbinder Sverige och Norge över Idefjorden vid Svinesund och utgör en viktig länk i det europeiska motorvägssystemet. För en av de mer väsentliga delarna av bron, nämligen bågens hjässa, förändrades produktionsprocessen jämfört med den planerade. Innan det sista segmentet i hjässan göts monterades stålstänger mellan båghalvorna. Därefter gjordes en reglering av krafterna i spännkablarna som stabiliserade båghalvorna vilket medförde att stålstängerna belastades. Det har sedan dess varit osäkert om denna avvikelse från den ursprungliga byggplanen kommer att leda till problem i framtiden på grund av långtidseffekter.

En finit elementmodell (FE-modell) av den nya Svinesundsbron har utvecklats av Plos och Movaffaghi (2004), inklusive en förenklad analys av uppförandet av bron. Denna modell har vidareutvecklats av Canovic och Goncalves (2005) och inkluderar det stegvisa utbyggnadsförloppet av bågen, samt materialmodeller som beskriver krypning och temperaturberoende.

Syftet med detta examensarbete var att förbättra och utveckla den redan befintliga FE-modellen och att utföra en förfinad analys av bågens hjässa, samt att ta långtidseffekter i beaktande. Modellen i detta examensarbete har uppdaterats genom att ta hänsyn till; den verkliga produktionen av hjässan, materialegenskaper så som krypning och krympning, samt en analys av brons hela livslängd. Med hjälp av tvärsnittskrafterna från analysen har en mer detaljerad undersökning av bågens hjässparti genomförts.

Det konstaterades att påverkan av krypning och krympning har en ogynnsam effekt på båghjässans tvärsnittsrespons i ett långtidsperspektiv. Även om effekterna på lång sikt har en negativ inverkan på hjässan, har de kritiska händelserna konstaterats inträffa under uppförandet av bågen. Gällande stålstängerna kunde det konstateras att normalkraften ökade med tiden på grund av de långtidseffekterna.

Efter en noggrannare analys av tvärsnittsresponsen och av infästningsområdet av stålstängerna, konstaterades att de aktuella spänningstillstånden inte kommer att orsaka några problem gällande den framtida responsen av båghjässan.

Nyckelord: Svinesund, Bro, Båge, Finita element, Långtidseffekter, Krympning, Krypning

Contents

Preface

This Master's thesis project was carried out at the Department of Civil and Environmental Engineering, Division of Structural Engineering at Chalmers University of Technology in Göteborg, Sweden. The work was performed during the period between January and June 2010.

The purpose of this Master's thesis project was to develop a FE-model of the New Svinesund Bridge with regard to long-term effects, with the emphasis to evaluate the long-term performance of the arch crown connection. The work in this Master's thesis was carried out as a part of a research project financed by the Swedish Road Administration (Vägverket).

Ass.Professor Mario Plos at Concrete Structures, Chalmers University of Technology was the examiner and Ph.D. student Hendrik Schlune at Concrete Structures, Chalmers University of Technology was the supervisor for this Master's thesis.

We would like to thank Ph.D. student Hendrik Schlune and Ass.Professor Mario Plos for their valuable support during the modeling process and the critical review of our report. We would also like to thank the staff at Vägverket for their support concerning the documentation of the bridge.

Finally, we would like to thank our opponents Karin Olsson and Josef Pettersson for their devotion and constructive criticism throughout the entire project.

Göteborg June 2010

Per Lindberg & Jonas Nilsson

Notations

Roman upper case letters

A_c	Cross-section of the concrete member
G_0	Instantaneous shear relaxation modulus
$G_R(t)$	Time dependent shear relaxation modulus
E_c	Reduced modulus of elasticity due to elastic analysis
E_{cm}	Modulus of elasticity
E_{ci}	Modulus of elasticity at an age of 28 days
$E_{ci}(t)$	Modulus of elasticity at an age of t days
$K_R(t)$	Time dependent bulk relaxation modulus
E_0	Young's modulus at $t = 0$
K_0	Instantaneous shear relaxation modulus
RH	Ambient relative humidity

Roman lower case letters

f_{ck}	Characteristic compressive strength
h	Notional size
f_{cm}	Mean compressive strength of concrete after 28 days
$f_{cm}(t)$	Mean compressive strength of concrete at an age of after t days
f_{ctm}	Mean tensile strength of concrete
s	Coefficient taking the cement into account
t	Age of concrete
t_s	Age of concrete at the beginning of the shrinkage (days)
t_0	Age of concrete at loading (days)
u	Perimeter of member exposed to the ambient air
f_{ct}	Tensile strength of concrete
f_{cc}	Compressive strength

Greek upper case letters

$\emptyset_0$	Notional creep coefficient

Greek lower case letters

α_G	Relaxation factor
α_K	Relaxation factor
$\beta_E(t)$	Function depending on the age t days
$\beta_{cc}(t)$	Time function
$\beta_s(t)$	Time function of shrinkage
β_{RH}	Factor considering the ambient relative humidity
β_{sc}	Coefficient depending on the type of cement
β_c	Coefficient describing creep development with time after loading
$\beta(f_{cm})$	Factor considering the concrete strength
$\beta(t_0)$	Factor considering the age of the concrete when loading
β_H	Coefficient depending on the humidity and the notional size

$\varepsilon_c(t)$	Concrete strain at time t
$\varepsilon_{ci}(t_0)$	Initial elastic strain at loading
$\varepsilon_{cc}(t)$	Creep strain at $t > t_0$
$\varepsilon_{cs}(t)$	Shrinkage strain
ε_{cs0}	Notional shrinkage coefficient
$\dot{\varepsilon}_i^{sw}$	Swelling strain rate
$\dot{\varepsilon}_i^{cs}$	Shrinkage strain rate
ε_i^{cs}	Shrinkage strain at time i
ε_c	Concrete strain
ε_s	Steel strain
v_0	Poisson's ratio at $t = 0$
$\sigma_c(t)$	Applied stress in concrete at time t
σ_c	Concrete stress
σ_s	Steel stress

1 Introduction

1.1 Background

The New Svinesund Bridge was opened for traffic in 2005 in connection with the 100 year dissolution of the union between Sweden and Norway. The new highway bridge connects Sweden and Norway over the Ide fjord at Svinesund and forms an important link in the European highway system. The design of the bridge was a result of an international architectural design contest where the winning design was an elegant and structurally demanding bridge due to the very slender arch form.

Due to its special design as one of the world's largest single-arched bridges, it was equipped with an advanced monitoring system in order to measure the real response of the bridge. The monitoring program was developed in collaboration between the Swedish Road Administration (Vägverket), the Royal Institute of Technology (KTH), the Norwegian Geotechnical Institute (NGI) and the Norwegian Road Administration (Statens Vegvesen).

At the division of Structural Engineering, Concrete Structures, at Chalmers University of Technology, a research project was initiated concerning bridge assessment and maintenance based on finite element (FE) analysis and field measurements, and where The New Svinesund Bridge was used as a case study. The FE-model used in the project was initially produced by the contractor for the bridge design, Bilfinger Berger (2004), and was converted to the FE-program ABAQUS by Plos, Movaffaghi (2004).

The FE-model has been further developed in two Master's thesis projects, Canovic, Goncalves (2005), and, Jonsson, Johnson (2007), and in a Licentiate thesis by Schlune (2009). The project by Canovic and Goncalves involved a development of the sequential construction of the arch, including creep and the development of Young's modulus with time. Schlune, Jonsson and Johnson used the measured data from the monitoring system to improve the accuracy of the original FE-model in their projects.

Recently the Swedish Road Administration initiated a new research project to further investigate the bridge. For one of the more essential parts of the bridge, the arch crown connection, the construction process was changed compared to the original plan. It was uncertain if this deviation in constructing the arch would lead to problems in the future. Therefore a need of an improved analysis of this particular part of the arch was identified.

1.2 Problem description

The arch was constructed using the cable-stayed cantilevering method and was, for construction purposes, divided into segments that were cast subsequently from both the Swedish and the Norwegian side. Before the last segment of the arch crown was cast, smooth surface steel bars were placed in between the arch halves. The forces in the temporary tendons supporting the arch halves were then reduced and the steel bars were loaded to prevent movements during the casting of the last segment. Early after the last segment was cast, the dismantling of the temporary cables started so that the construction of the carriageways could proceed.

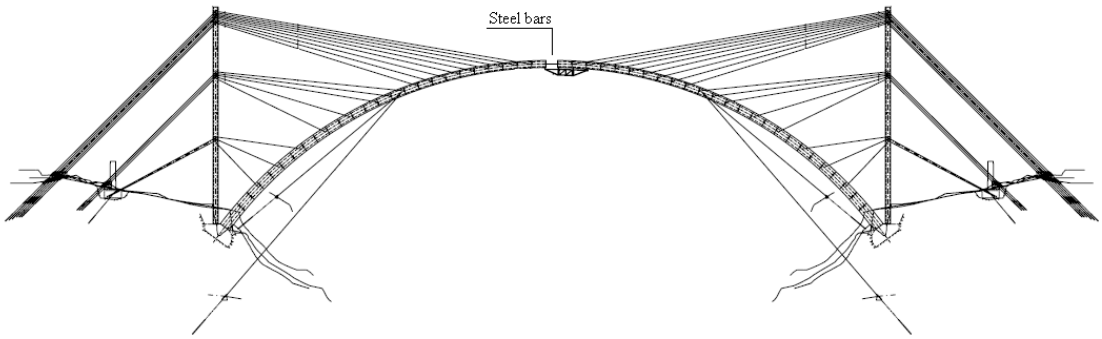

Figure 1.1 The cable-stayed arch divided in segments and with the steel bars connecting the arch halves. Adopted from Vägverket (2007)

When the steel bars were loaded, concentrated compressive forces were acting on the adjacent segments. Since these segments had not developed their full strength, there is a risk that this concentrated force has, or will, result in crushing or splitting in the disturbed region close to the attachment area. Due to the smooth surface of the bars, full interaction with the surrounding concrete is not expected, and therefore will this concentrated force increase due to long-term effects in the concrete.

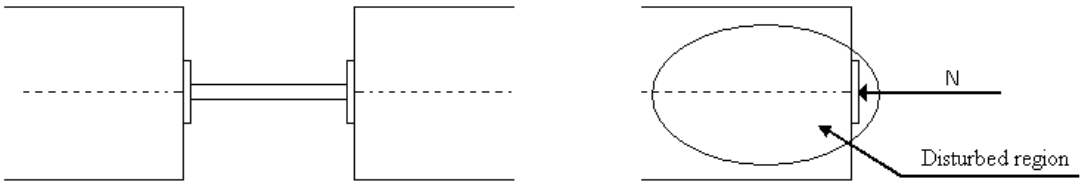

Figure 1.2 The attachment area between the steel bars and the concrete segments.

Another effect of the steel bars is that a part of the normal force in the crown segment will pass through the bars instead of through the reinforced concrete section. A problem that could occur, due to long-term effects, is that a larger part of the normal force will be redistributed to the steel bars with time. This change of force distribution might lead to that the normal force acting on the concrete section will not remain big enough to maintain the entire cross-section in a compressed state and the risk of tensile cracks will increase.

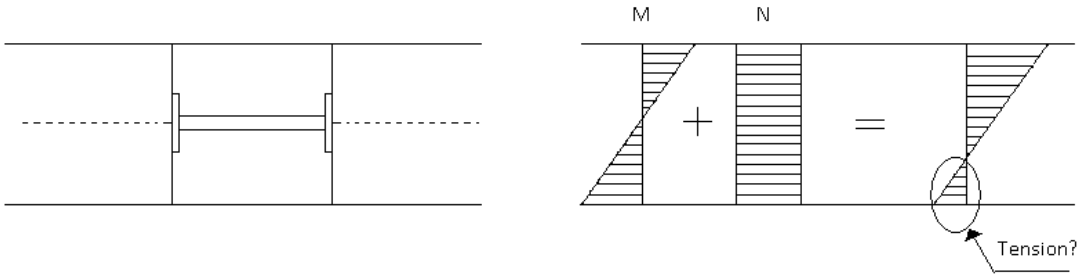

Figure 1.3 The steel bar casted in concrete and principle figure of the stress distribution in the crown segment.

1.3 Aim and objectives

The aim of this study was to improve the already existing FE-model developed by Canovic and Goncalves, and to perform an improved analysis of the arch crown connection. The development and improved analysis should include long-term effects such as creep and shrinkage. An FE-model, including the effect of creep, made by Canovic and Goncalves was improved to be able to analyze longer time periods. It was complemented with an FE-model including shrinkage to improve the modeling of the long-term response. The objective was to draw conclusions concerning force and stress distribution in the arch crown based on the results from the FE-analysis, and to predict how this will effect the future performance of the bridge.

1.4 Scope of study

The FE-model created by Canovic and Goncalves was constructed before the completion of the real bridge. Therefore, the input data for the late construction phases were in some parts based on assumptions. This FE-model was improved by simulating the construction of the arch based on complete construction documents, by material properties based on test data for all segments, and to improve the model in the area of the arch crown, where steel bars were included. A further development of the analysis of the bridge was made by creating a FE-model taking shrinkage effects into account. The sectional forces from the FE-analysis were used to evaluate the stress and force distribution in the crown segment in the long-time perspective. The capacity of the arch crown section has been analyzed in order to investigate if any critical events might occur during its life time. The disturbed regions in the attachment area have been evaluated by a more detailed FE-model of this particular region.

2 The New Svinesund Bridge

2.1 Description of the bridge

The New Svinesund Bridge is a single-arched highway bridge joining Sweden and Norway over the Ide fjord. The bridge consists of a continuous steel superstructure carried by a concrete substructure and a concrete arch. The bridge has a total length of 704m measured between the land embedments and has a largest span of 247m between the arch abutments.

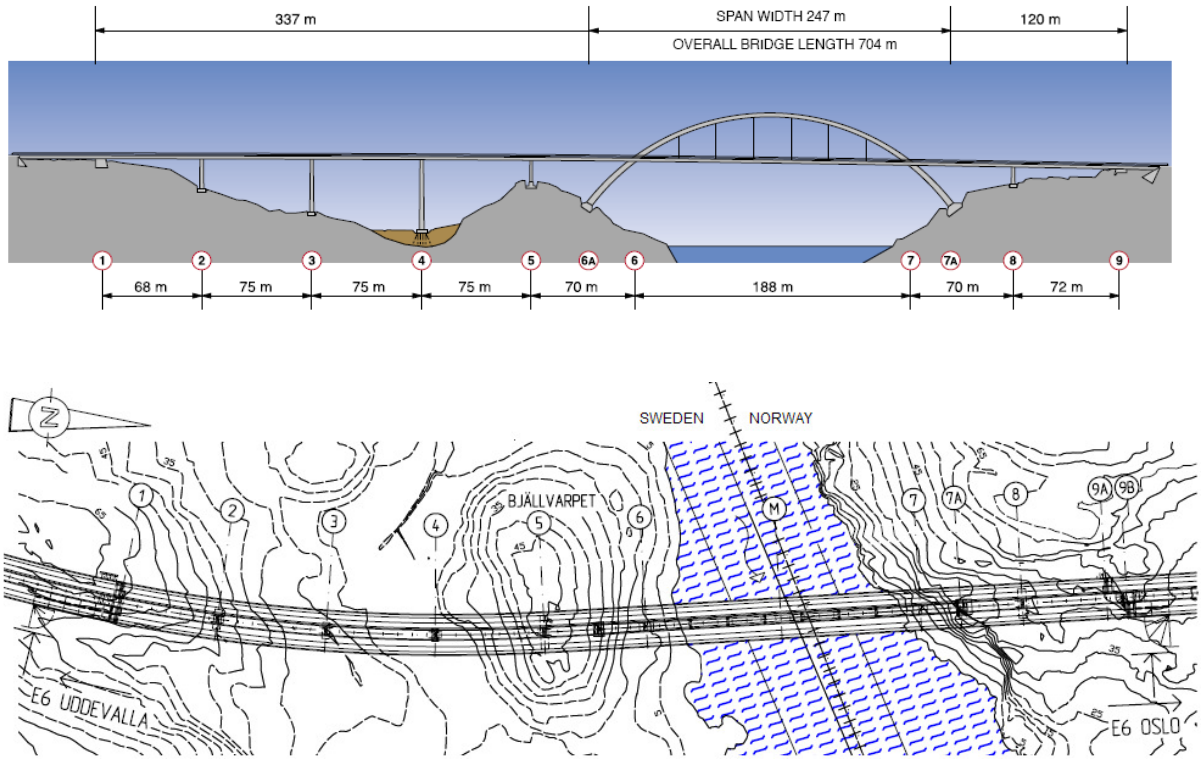

Figure 2.1 Drawings showing the New Svinesund Bridge in elevation and in plan. Vägverket (2007)

2.1.1 The superstructure

The steel superstructure is divided in two separate box-girders, one for each carriageway. The two carriageways are connected to each other by integrated cross-girders located only at the supporting columns and at the arch hangers. The bridge decks are designed as orthotropic plates and the inside of the steel boxes are stiffened with both longitudinal and lateral diaphragms. The total width of the superstructure is 28,2m including both carriageways and the gap in between them.

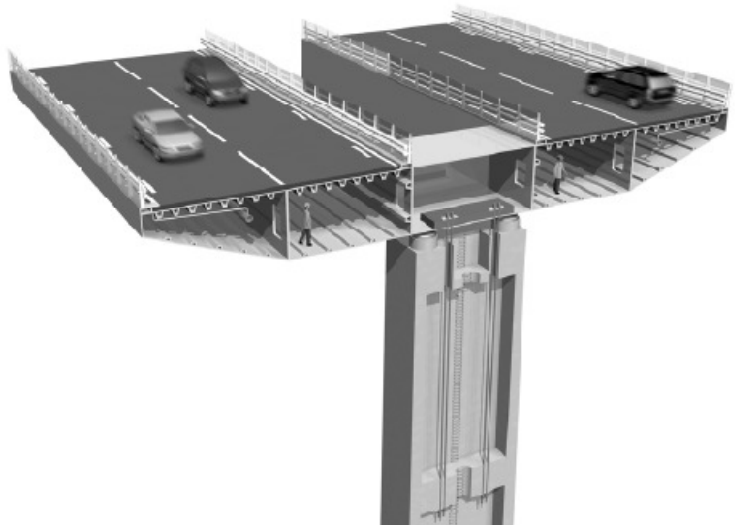

Figure 2.2 Section of the carriageways showing the cross-girders and the longitudinal stiffeners of the orthotropic plate. Vägverket (2007)

The superstructure was prefabricated in Germany and was delivered to the building site in segments. The carriageways were erected by using three different methods. The bridge decks on the Swedish side of the fjord were launched from the land embedment. On the Norwegian side the bridge decks was lifted into place by cranes. Finally, the part of the deck hanging from the arch was lifted into position from barges on the fjord.

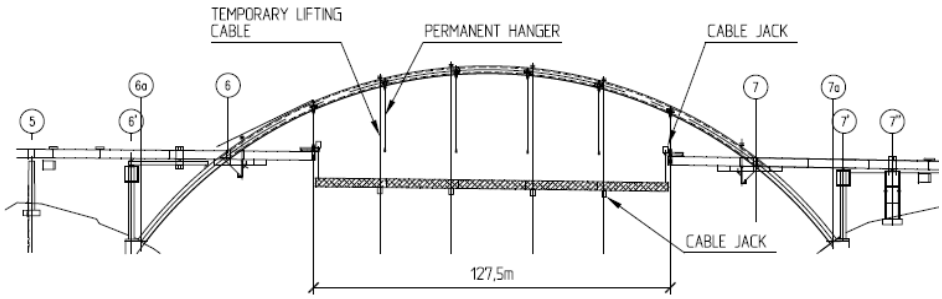

Figure 2.3 The lifting procedure of the bridge deck. Vägverket (2007)

2.1.2 The arch

The arch is a slender reinforced concrete arch constructed using the cable-stayed cantilevering method. It has a circular shape with a radius of 154m and has a rectangular box cross-section that tapers in both height, width and wall thickness from the abutments towards the arch crown.

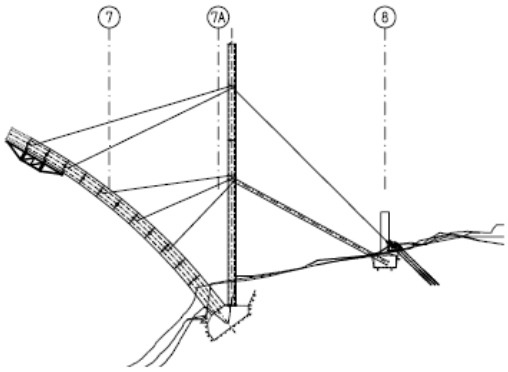

Figure 2.4 The principle procedure of the cable-stayed cantilever method. Vägverket (2007)

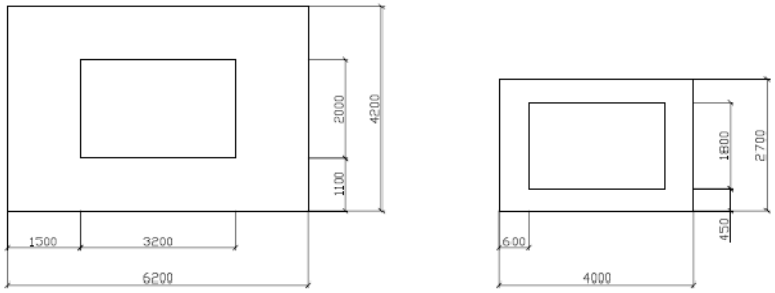

Figure 2.5 Typical cross-sections of the arch due to the tapered shape. The left section is at the abutments while the right one is close to the crown.

The superstructure is suspended from the arch with 6 pairs of steel hangers. To provide the arch with lateral stability, the carriageways are connected to the arch with post-tensioned tendons at the level of the road decks.

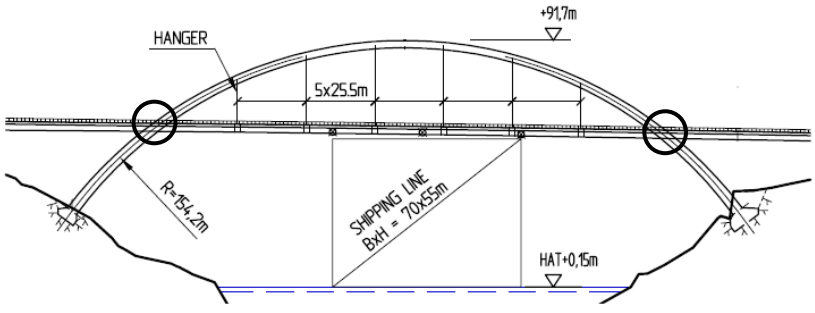

Figure 2.6 Geometry of the arch and its connection to the superstructure, where the marked areas shows the position of the post-tensioned tendons. Vägverket (2007)

2.1.3 The substructure

The substructure consists of two land embedments and five intermediate column supports. The substructure is made of ordinary reinforced concrete and due to the varying landscape underneath the bridge the height of the supports differs from 11m to 47m.

Due to the architectural vision to create a slender appearance of the bridge, the supporting columns were not allowed to be wider than the gap between the carriage ways. These geometric conditions created challenges for the connection between the supporting columns and the carriageways. In these connections large uplifting forces can occur due to the eccentricity of the traffic load. To handle these forces, vertical prestressed tendons were installed and anchored to prefabricated cross-beams inside the columns.

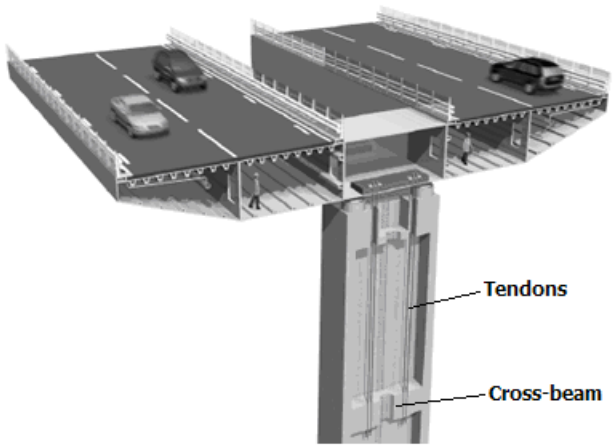

Figure 2.7 Cross-section of the supports showing the prestressed tendons and the cross-beam where the tendons were anchored. Vägverket (2007)

2.2 Construction of the arch

Due to the heavy shipping traffic on the Ide fjord traditional scaffolding was not possible when constructing the arch. Instead the arch was constructed using the cable-stayed cantilevering method with a specially designed self-climbing formwork. For construction purposes the arch was divided into segments that were cast subsequently from both the Swedish and the Norwegian side. In total 53 segments including the abutments were cast to complete the bridge.

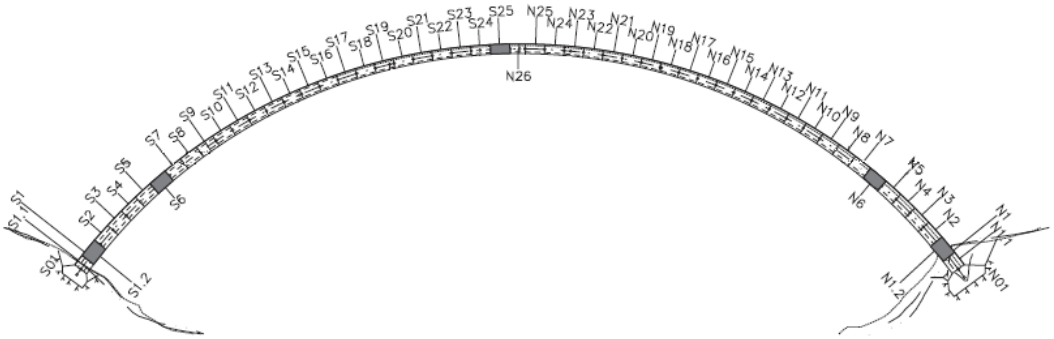

Figure 2.8 The arch divided in segments. James and Karoumi (2003)

2.2.1 Launching procedure

The construction started with the foundation on both the Swedish and Norwegian side and each of the following segments were cast successively with help of the self-climbing formwork. The first three segments were cast with help of ordinary scaffolding and the following segments of the cantilevering structure were supported by temporary steel tendons via auxiliary towers. The temporary tendons were fixed to the towers at three different levels and were then back-anchored in the bedrock behind the towers. To stabilize the arch laterally during the construction face, additional tendons were fixed on each side of the arch.

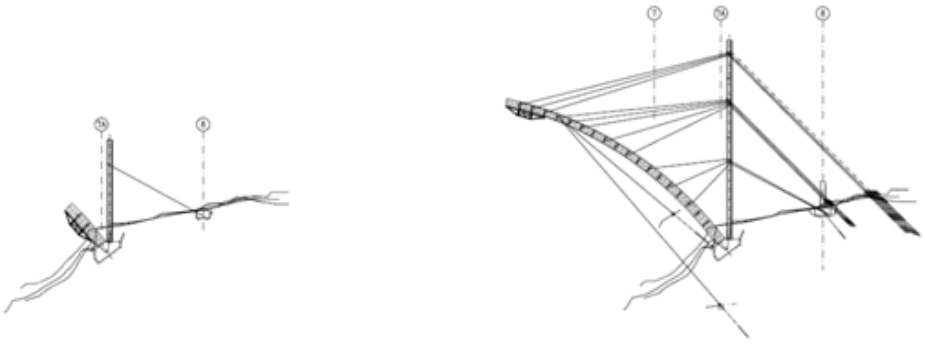

Figure 2.9 The left figure shows the stage when the arch was supported by ordinary scaffolding and the right figure when the arch was supported by temporary tendons. Vägverket (2007)

2.2.2 Casting procedure

Due to the tapered shape of the arch and the variation of wall thickness, a specially designed formwork was developed, that was easy to reconstruct with regard to the sectional changes. The formwork had an underlying load carrying truss-girder that was attached to the previously cast segment, and the movement of the formwork into the next position was achieved by hydraulic devises. The design of the formwork, with an underlying load carrying structure also enabled prefabricated reinforcement cages to be put in place. Before casting of the new segment the deformation due to self-weight was calculated, and the temporary stay-cables was stressed so that the newly cast segment should deform in to its correct position. In this way the final form of the arch was controlled so that the intended shape was obtained.

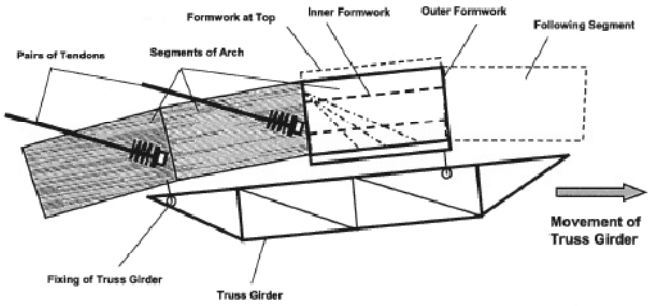

Figure 2.10 Movement of the truss girder into position for the next segment. Bilfinger Berger (2003)

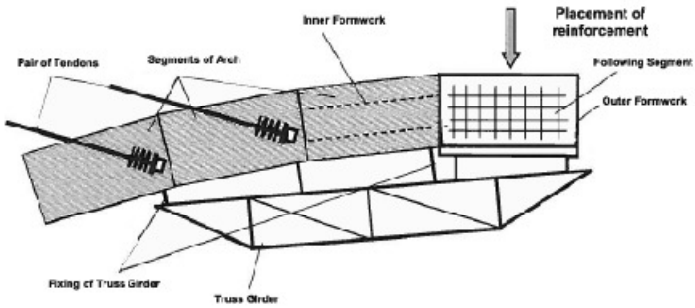

Figure 2.11 Outer formwork in position and the prefabricated reinforcement cage is placed. Bilfinger Berger (2003)

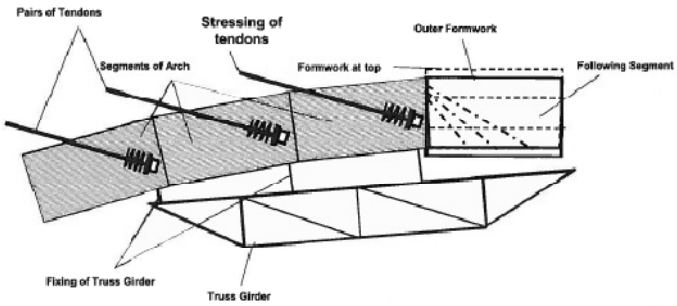

Figure 2.12 Tendons is placed and stressed in the previous segment before casting of the following segment. Bilfinger Berger (2003)

To provide the construction of the arch with material supplies such as reinforcement and concrete, a cable crane was mounted across the fjord. The crane had a working length of 330m and the material was carried by mechanical powered carriages. The cable towers were made of trusses and could be tilted ±10m sideways which made it possible to serve the entire working area for the arch. The first four casting stages on each side of the fjord were cast using a concrete pump while the other stages were cast using the cable crane and a concrete skip.

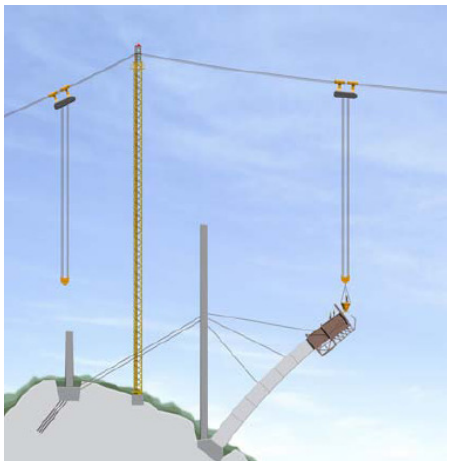

Figure 2.13 Figure showing the principle how the cable crane was used to transport material to the working site of the arch. James and Karoumi (2003)

2.2.3 Closing procedure

The last casting stage for the arch was to cast the crown segment that joins the two halves together. The first step in the closing procedure was to install two steel bars in between the adjacent segments, followed by a decrease of tendon forces in the upper cables in order to activate and make the bars load carrying. The reason for inserting the bars was to fixate the arch halves in the right position and to eliminate the possibility of movements during casting of the last segment. The bars were circular steel tubes with a diameter of 219,1mm, a thickness of 6,3mm and were filled with concrete. The bars were placed on top of L-shaped steel plates, which were bolted to the adjacent segments. To create a good contact between the bars and the segments expanding grout was used.

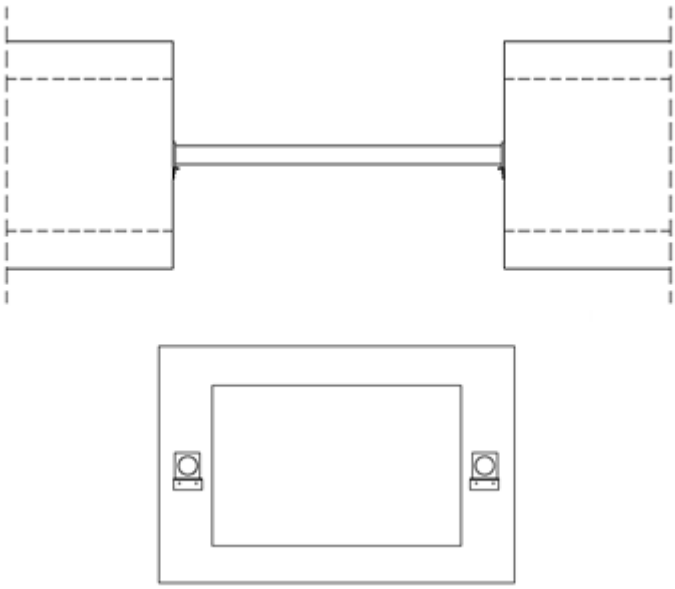

Figure 2.14 Position of the steel bars between the arch halves.

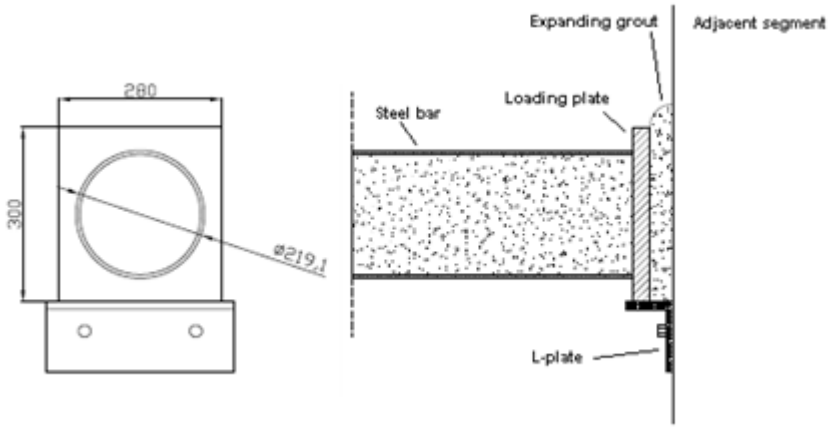

Figure 2.15 Connection between the steel bars and the adjacent segments.

When the concrete in the crown segment had obtained the necessary compressive strength the dismantling of the temporary stay cables started according to a predetermined programme.

3 Material properties of concrete

The material properties of concrete have a very complex nature and the development of these depends on several different parameters, described further in this chapter. Empirical expressions for the material properties and their development with time are described in CEB/FIP Model Code 1990, see Appendix A. These expressions have been used in the calculations concerning the material properties in this thesis.

3.1 Development of compressive strength

Newly cast concrete has almost fluid properties but changes phase early after the start of the hydrating process, and the concrete gradually changes into a hard material with initially low compressive strength. The rate of hardening is effected by temperature, type of cement, admixtures and curing conditions. After some time the concrete starts to develop its strength. The development of the strength has a rapid increase in the beginning of the hydrating process and will later grow slowly during time. This property of concrete strength growth makes the material sensitive to early age loading. Illston, Domone (2008)

3.1.1 Compressive strength according to CEB/FIP Model Code 1990

The development of the mean compressive strength, $f_{cm,}$ is dependent of type of cement, ambient temperature and curing conditions. For a mean temperature of 20°C the relative compressive strength for concrete can be calculated as a function of time, according to (3.1). The time function $\beta_{cc}(t)$ can be calculated from equation (3.2) and takes the effect of time and the cement type into account.

$$f_{cm}(t) = \beta_{cc}(t) f_{cm} \tag{3.1}$$

with

$$\beta_{cc}(t) = e^{s\left[1-\left(\frac{28}{t/t_1}\right)^{\frac{1}{2}}\right]} \tag{3.2}$$

where

$f_{cm}(t)$ mean compressive strength at an age of *t* days (MPa)

$\beta_{cc}(t)$ time function

f_{cm} strength after 28 days (MPa)

t age of concrete (days)

t_1 1 day

s coefficient taking the type of cement into account
s = 0,20 for rapid hardening high strength cement RS
s = 0,25 for normal and rapid hardening cement N and R
s = 0,38 for slow hardening cement SL.

3.2 Development of tensile strength

The tensile strength of concrete depends mainly on the same parameters which influence the compressive strength of concrete. The tensile strength shows a greater variation compared to the compressive strength. This is due to the fact that the tensile strength is dependent on the shape and surface texture of the aggregates.

3.2.1 Tensile strength according to CEB/FIP Model Code 1990

With a specified characteristic compressive strength f_{ck}, the mean value of the tensile strength f_{ctm} can be estimated according to

$$f_{ctm} = f_{ctk0,m} \cdot \left(\frac{f_{ck}}{f_{ck0}}\right)^{2/3} \tag{3.3}$$

with

$$f_{ck} = f_{cm} - \Delta f \tag{3.4}$$

where

f_{ctm} mean tensile strength (MPa)

$f_{ctk0,m}$ 1,40 MPa

f_{ck} characteristic compressive strength (MPa)

f_{ck0} 10 MPa

f_{cm} mean compressive strength (MPa)

Δf 8 MPa

3.3 Development of the modulus of elasticity

The modulus of elasticity also increases with increasing compressive strength, but the development of the modulus is more rapid than for the compressive strength. Due to the fact that the volume of concrete is, to a great amount, occupied by aggregates, the properties of the aggregates will have a significant influence of the modulus of elasticity.

3.3.1 Modulus of elasticity according to CEB/FIP Model Code 1990

The modulus is dependent on the hardening of the concrete which is described in terms of the characteristic strength f_{ck}.

$$E_{ci} = E_{c0}[\frac{f_{ck}+\Delta f}{f_{cm0}}]^{1/3} \quad (3.5)$$

where

E_{ci} modulus of elasticity at an age of 28 days (MPa)

f_{ck} characteristic compressive strength (MPa)

Δf 8 MPa

f_{cm0} 10 MPa

E_{c0} 2,15*10^4 MPa

When only an elastic analysis of a concrete structure is carried out, a reduced modulus of elasticity according to equation (3.6) should be used.

$$E_c = 0{,}85 \cdot E_{ci} \quad (3.6)$$

When the age of the concrete differs from 28 days the modulus of elasticity can be estimated as:

$$E_{ci}(t) = \beta_E(t) \cdot E_c \quad (3.7)$$

with

$$\beta_E(t) = [\beta_{cc}(t)]^{0,5} \quad (3.8)$$

where

$E_{ci}(t)$ modulus of elasticity at an age of *t* days

E_{ci} modulus of elasticity at an age of 28 days

E_c reduced modulus of elasticity at an age of 28 days

$\beta_E(t)$ function depending on the age *t* days

$\beta_{cc}(t)$ time function according to equation (3.2)

3.4 Long term effects

In addition to the development of material strength and stiffness, the response of concrete is time dependent due to effects originating from volume changes such as creep and shrinkage. These volume changes lead to development of stresses in the material. The total strain for a uniaxially loaded member subjected to a constant stress at a concrete age of *t* days can be determined according to

$$\varepsilon_c(t) = \varepsilon_{ci}(t_0) + \varepsilon_{cc}(t) + \varepsilon_{cs}(t) \tag{3.9}$$

where

$\varepsilon_{ci}(t_0)$ initial strain at loading

$\varepsilon_{cc}(t)$ creep strain at time $t > t_0$

$\varepsilon_{cs}(t)$ shrinkage strain

3.4.1 Shrinkage

Shrinkage is the decrease of concrete volume with time due to changes in the moisture content and chemical changes inside the concrete. The shrinkage strain is not dependent on the state of stresses and will develop independently of loading. Shrinkage of concrete starts already during the hardening process and reaches its final value after long time. The shrinkage strain of concrete is composed of two parts, autogenous and drying shrinkage.

Autogenous shrinkage takes place inside the concrete during hardening and develops mainly during the first days after casting. The autogenous shrinkage arises due to chemical reactions between water and cement inside the concrete, without any moisture exchange to the surroundings. The magnitude of autogenous shrinkage is less than the drying shrinkage but can be more significant with small water/cement ratios, such as in high strength concrete.

The drying shrinkage on the other hand develops slowly with time and is dependent on the moisture exchange with the ambient environment. In normal strength concrete with relatively high water/cement ratio a large part of the water is not consumed during the hydration process and will remain in the pores of the hardened concrete. When the concrete then is exposed to a dry environment the water starts to dry out which leads to a decrease of concrete volume. Drying shrinkage has the most significant contribution to the total shrinkage. Important parameters that influence the drying shrinkage are the composition of the concrete, the humidity of the surroundings and the size of the exposed surfaces in relation to the volume.

3.4.1.1 Shrinkage according to CEB/FIP Model Code 1990

The calculation of the total shrinkage strain, (see Appendix B) $\varepsilon_{cs}(t, t_s)$ may be calculated as

$$\varepsilon_{cs}(t, t_s) = \varepsilon_{cso} \cdot \beta_s(t - t_s) \tag{3.10}$$

where

β_s time function

ε_{cso} notional shrinkage coefficient

t age of concrete (days)

t_s age of concrete at the beginning of shrinkage (days)

with

$$\varepsilon_{cso} = \varepsilon_s(f_{cm})\beta_{RH} \tag{3.11}$$

where

β_{RH} factor considering the ambient relative humidity

with

$$\varepsilon_s(f_{cm}) = [160 + 10\beta_{sc}(9 - \frac{f_{cm}}{f_{cmo)}}] \cdot 10^{-6} \tag{3.12}$$

where

f_{cm} mean compressive strength at an age of 28 days (MPa)

f_{cmo} 10 MPa

β_{sc} coefficient depending on the type of cement

$\beta_{Sc} = 8$ for rapid hardening high strength cement RS

$\beta_{Sc} = 5$ for normal or rapid hardening cement N and R

$\beta_{Sc} = 4$ for slowly hardening cement SL

$$\beta_{RH} = \text{-}1.55\beta_{sRH} \qquad 40\% \leq \text{RH} < 99\%$$

$$\beta_{RH} = +0.25 \qquad \text{RH} \geq 99\% \tag{3.13}$$

where

$$\beta_{sRH} = 1 - \left(\frac{RH}{RH_0}\right)^3 \tag{3.14}$$

with

RH ambient relative humidity (%)

RH_0 100%

The development of shrinkage with time is given by

$$\beta_s(t - t_s) = [\frac{(t-t_s)/t_1}{350(h/h_0)^2 + (t-t_s)/t_1}]^{0.5} \tag{3.15}$$

with

$$h = \frac{2 \cdot A_c}{u} \tag{3.16}$$

where

h notional size

A_c cross-section of member

u perimeter of member exposed to the ambient air

t_1 1 day

h_0 100mm

3.4.1.2 Implementation of shrinkage in ABAQUS

In order to model the shrinkage behaviour of concrete in ABAQUS the option *SWELLING was applied in the material specification. This option was used to specify the time-dependent shrinkage behaviour of the concrete. The swelling behaviour is defined in tabular form and requires that the material is defined as linear elastic, and the swelling option can only be used in combination with the visco-elastic material model according to 3.4.2.

When defining the swelling in tabular form, the strain rate, temperature and field variables are necessary as input Appendix C. The strain rate is defined as a linear variation according to

$$\dot{\varepsilon}_i^{sw} = \dot{\varepsilon}_i^{cs} = 3 \cdot \frac{\varepsilon_i^{cs} - \varepsilon_{i-1}^{cs}}{t_i - t_{i-1}} \tag{3.17}$$

where

$\dot{\varepsilon}_i^{sw}, \dot{\varepsilon}_i^{cs}$ strain rate

ε_i^{cs} strain at time step i

t_i age of concrete at time step i

The strain ε_i^{cs} at different time steps are calculated according to CEB/FIP Model Code 1990 in section 3.4.1.1.

3.4.2 Creep

The definition of creep is a load dependent strain that develops with time. The magnitude of the creep strains can be several times larger than the elastic strains caused by the load. Creep deformations grow with time and will be fully developed after a very long time, approximately 70 years CEB-FIP (2009). Therefore, it is of big importance to take the creep deformations into account in the analysis of concrete structures.

Factors that highly effect the development of creep are the magnitude and the duration of the load, and the age of concrete when loaded. The creep deformations can be more than doubled when concrete is loaded at early age compared to loading at 28 days. This is due to material properties, such as the rapid strength growth of young concrete. Other factors that also have big influence on creep are the composition of the concrete, the ambient relative humidity and the size and shape of the section. The shape dependency of creep is mostly related to the fact that different shapes have different drying speeds. This leads to differences in the creep propagation for different sections.

Creep deformations can be seen as summation of reversible and irreversible deformations. The reversible deformations are called delayed elastic creep while the irreversible are called viscous creep deformations. This means that when the concrete member is unloaded the elastic creep will recover but the viscous creep deformation will remain.

Creep is defined as a deformation with time under more or less constant stress. The opposite phenomenon, when the strain is constant over time due to for example boundary conditions, the stress decrease is called relaxation. According to the Comite' Euro-International du Béton (1993) there are several creep functions to describe each factor effecting the creep of concrete, which in turn are combined to describe the complex nature of the creep behavior.

3.4.2.1 Creep according to CEB/FIP Model Code 1990

The creep coefficient may be calculated (see Appendix D) as

$$\emptyset(t, t_0) = \emptyset_0 \cdot \beta_c(t - t_0) \tag{3.18}$$

where

$\emptyset_0$ notional creep coefficient

β_c coefficient describing creep development with time after loading

t age of the concrete at the moment considered (days)

t_0 age of concrete at loading (days)

The notional creep coefficient can be estimated as

$$\emptyset_0 = \emptyset_{RH} \cdot \beta(f_{cm}) \cdot \beta(t_0) \tag{3.19}$$

where

$\emptyset_{RH}$ factor considering the relative humidity

$\beta(f_{cm})$ factor that consider the concrete strength

$\beta(t_0)$ factor considering the age of concrete when loaded

with

$$\emptyset_{RH} = 1 + \frac{1 - RH/100}{0{,}46 \cdot \sqrt[3]{h/h_0}} \tag{3.20}$$

where

RH ambient relative humidity (%)

h notional size of the member according to equation (3.16)

h_0 100 mm

with

$$\beta(f_{cm}) = \frac{5.3}{\sqrt{f_{cm}/f_{cm0}}} \qquad \text{f}_{\text{cm}} \text{ in MPa} \tag{3.21}$$

$$\beta(t_0) = \frac{1}{0{,}1 + (t_0/t_1)^{0{,}20}} \tag{3.22}$$

where

t_0 age when load is applied (days)

f_{cm} mean compressive strength of the concrete at the age of 28 days

f_{cm0} 10 MPa

RH ambient relative humidity

t_1 1 day

The development of creep coefficient during time is defined as the time function $\beta(t-t_0)$.

$$\beta(t-t_0) = \left[\frac{(t-t_0)/t_1}{\beta_H+(t-t_0)/t_1}\right]^{0,3} \quad (3.23)$$

where

t age of the concrete (days)

t_1 1 day

β_H coefficient depending on the relative humidity and the notional size

with

$$\beta_H = 1{,}5[1+(0{,}012RH)^{18}]h_0 + 250 \leq 1500 \quad (3.24)$$

3.4.2.2 Implementation of creep in ABAQUS with relaxation test data

In the Master's thesis by Canovic and Goncalves different ways of modelling the creep behaviour of concrete were investigated, and it was found that the most proper way of modelling creep was to model the material as viscoelastic in the time domain using the option *VISCO. This thesis was a continuance of the model produced by Canovic and Goncalves therefore this material model was used.

The viscoelastic material is defined by a Prony series expansion of the dimensionless shear relaxation modulus $g_R(t)$ and the dimensionless bulk relaxation $k_R(t)$ modulus, according to Hibbit, Karlsson and Sorensen Inc. (2002):

$$g_R(t) = 1 - \sum_{i=1}^{N} g_i^P\left(1 - e^{\frac{-t}{\tau_i^G}}\right) \quad (3.25)$$

$$k_R(t) = 1 - \sum_{i=1}^{N} k_i^P\left(1 - e^{\frac{-t}{\tau_i^k}}\right) \quad (3.26)$$

where

$N, g_i^P, \tau_i^G, k_i^P, \tau_i^k$ are material constants and t is time

The dimensionless shear relaxation modulus $g_R(t)$ and the dimensionless bulk relaxation modulus $k_R(t)$ are defined as

$$g_R(t) = \frac{G_R(t)}{G_0} \quad (3.27)$$

$$k_R(t) = \frac{K_R(t)}{K_0} \quad (3.28)$$

where

$G_R(t)$ time dependent shear relaxation modulus

$K_R(t)$ time dependent bulk relaxation modulus.

These parameters are obtained for linear elastic materials by multiplying the instantaneous relaxation moduli with a dimensionless relaxation factor such that

$$G_R(t) = \alpha_G \cdot G_0 \tag{3.29}$$

$$K_R(t) = \alpha_K \cdot K_0 \tag{3.30}$$

where

α_G the dimensionless relaxation function which is ≤ 1

α_K the dimensionless relaxation function which is ≤ 1

with

$$G_0 = \frac{E_0}{2 \cdot (1+\nu_0)} \tag{3.31}$$

$$K_0 = \frac{E_0}{3 \cdot (1-2 \cdot \nu_0)} \tag{3.32}$$

where

G_0 instantaneous shear relaxation modulus

K_0 instantaneous bulk relaxation modulus

E_0 Young's modulus at $t = 0$

ν_0 Poisson's ratio at $t = 0$

By combining equations (3.27) with (3.29) and (3.28) with (3.30), similarities can be identified compared to how the creep behaviour is taken into account by an effective modulus of elasticity. The dimensionless relaxation function is therefore defined as

$$g_R(t) = \frac{G_R(t)}{G_0} = \frac{\alpha_G . G_0}{G_0} = \alpha_G = \frac{1}{(1+\emptyset(t,t_0))} \tag{3.33}$$

$$k_R(t) = \frac{K_R(t)}{K_0} = \frac{\alpha_K . K_0}{K_0} = \alpha_K = \frac{1}{(1+\emptyset(t,t_0))} \tag{3.34}$$

where

$\emptyset(t, t_0)$ creep coefficient according to equation (3.18)

The values for $g_R(t)$ and $k_R(t)$ were inserted into ABAQUS in tabular form for different time steps, see Appendix E. Through the non-linear least-square fit, the parameters in the Prony series in equations (3.25) and (3.26) were calculated.

3.4.3 Different calculation approaches of creep under varying stress.

The creep strain is defined by a creep coefficient which relates the creep strain to the instantaneous elastic strain according to

$$\varepsilon_{cc}(t, t_0) = \emptyset(t, t_0) \cdot \frac{\sigma_c(t)}{E_{cm}} \tag{3.35}$$

with

$\emptyset(t, t_0)$ creep coefficient according to equation (3.18)

$\sigma_c(t)$ applied stress at time t

E_{cm} modulus of elasticity

Where the $\varepsilon_{cc}(t, t_0)$ is the creep deformation starting from time, t_0, to the actual time, t, of interest. The total strain due to loading can be calculated by adding the creep strain to the instantaneous elastic strain.

$$\varepsilon_c(t) = \frac{\sigma_c(t)}{E_{cm}} + \emptyset(t, t_0) \cdot \frac{\sigma_c(t)}{E_{cm}} \tag{3.36}$$

The effect of creep can be seen to have a softening influence on the concrete since the deformations increases with time. Therefore an effective modulus of elasticity, which decreases with time, can be defined as a function of the creep coefficient.

$$E_{c,ef}(t, t_0) = \frac{E_{cm}}{(1+\emptyset(t,t_0))} \tag{3.37}$$

Where the total deformation is now described as

$$\varepsilon_c(t) = \frac{\sigma_c(t)}{E_{c,ef}(t,t_0)} \tag{3.38}$$

In reality the concrete stress is not constant, but varies in time. If the concrete stress consists of stress components applied at different time, each stress component will result in one unique creep function that adds to the total creep deformation. There exist different methods to calculate the creep deformations in cases when the concrete stress varies with time, where some of the more common methods are described in the following parts.

3.4.3.1 The effective modulus of elasticity based on the first creep function

The simplest approach of estimating the creep deformation under varying stress is to consider the creep function from the moment when the structure first was loaded. This approach is convenient since the conventional design methods can be used as for the case with constant stress. The concrete age, t_0, should be taken as the age when the first load was applied. It means that only one creep function is used in the calculations, that of the first load.

$$\varepsilon_{cc}(t,t_0) = \emptyset(t,t_0) \cdot \frac{\sum_i \sigma_i}{E_{cm}} \tag{3.39}$$

This method can be used to approximate creep at any time when the loading history is unknown. It also gives reasonable approximations for structures with dominating self weight, and where the entire self weight is applied at the same time. In cases when the concrete stress decreases with time, the creep deformation will be underestimated, and if the concrete stress increases with time the creep deformation will be overestimated.

3.4.3.2 The effective modulus of elasticity based on several creep functions

This is a method that takes several creep functions and their associated stress change into account in an approximate way. Each stress component results in one unique creep function and where these are approximated by an effective creep coefficient, $\emptyset_{ef}(t,t_0)$. The effective creep coefficient is a weighted average of the creep coefficients and its corresponding stress components.

$$\emptyset_{ef}(t,t_0) = \frac{\sum_i \emptyset_{i(t,t_i)} \cdot \sigma_{ci}}{\sum_i \sigma_i} \tag{3.40}$$

Where the creep strain can be calculated as

$$\varepsilon_{cc}(t,t_0) = \emptyset_{ef}(t,t_0) \cdot \frac{\sigma_c}{E_{cm}} \tag{3.41}$$

3.4.3.3 The method of superposition

For the method of superposition, each stress component is assumed to result in one unique creep function. The creep function will develop independently of all other creep functions and can thereby be superimposed. This way of calculating the creep deformations is the most accurate of the described methods. In equation (3.42) it is shown how the creep strain is calculated based on the superposition method.

$$\varepsilon_{cc}(t,t_0) = \sum_i \emptyset(t,t_i)_i \cdot \frac{\sigma_{ci}}{E_{cm}} \tag{3.42}$$

Where $\emptyset(t,t_0)_i$ is the unique creep function associated with the stress component, σ_{ci}.

4 Finite element model

The FE-model presented in this thesis was a continuation of a FE-model created by Plos, Movaffaghi (2004) which was further developed by Canovic, Goncalves (2005).

The model produced by Plos and Movaffaghi was based on a FE-model from the bridge contractor, Bilfinger Berger (2004). The contractor supplied the authors with input data files from the FE-model used in the bridge design, complemented with design and construction documents. These files were converted and adopted to the FE-software ABAQUS, see Hibbitt, Karlsson and Sorensen Inc. (2002). In addition to the structural model, Plos and Movaffaghi also developed a simulation of the arch launching procedure.

Canovic and Goncalves further developed the model of the bridge and performed a more detailed analysis of the arch launching. The modelling intended to include the development of Young's modulus with time, temperature loads on the structure, and viscoelastic material properties to be able to consider the effect of creep.

In this thesis further improvements of the FE-model have been performed:

- Updates of the launching procedure of the arch were made concerning casting dates, together with changes of forces in the temporary tendons according to construction documents, see Appendix G.
- Individual material properties for each segment were included, according to documents from laboratory testing of concrete specimens taken from the real structure, see Appendix F.
- The steel bars in the arch crown were implemented to be able to study the force distribution in this particular area of the arch.
- Due to problems combining both creep and shrinkage behaviour in the same FE-model, a new model was developed to take the shrinkage behaviour into account. In this new model only the stiffness of the materials were taken into account without any gravity loads. This modification was made with the intention to superimpose the results from the creep and the shrinkage model.
- The model was improved to be able to analyse the entire service life of the bridge regarding long-term effects.

4.1 Description of the FE-model of the bridge

The already existing input file of the model was modified using a text editor. The input file was divided in two parts of data, model data and history data which is the analysis part.

The model data specifies the model with geometry and material. This part defines the nodes, elements, element properties, material properties, boundary conditions and other data that specifies the model.

The second part defines the history of the model. The history is divided in steps, where each step describes the particular event that occurs. The history data also defines the type of analysis that should be performed, type of action the model is subjected to, control parameters for time integration and loading, together with the desired output for each step.

4.1.1 Geometry

The node coordinates are defined in a right-handed three-dimensional Cartesian coordinate system. The origin of the coordinate system is centred under the midpoint of the arch, at level ±0 approximately at sea level. The system has a horizontal xy-plane with the x-axis pointing along the arch and positive in the direction towards Norway. The y-axis is oriented in the transversal direction pointing in eastern direction while the z-axis is positive down-wards towards the water.

The geometry is represented in the model by nodes and elements. The elements are defined between the nodes and together they build up a structure representing the bridge. The model of the bridge (Figure 4.1) consists of an arch (Figure 4.2), temporary tendons and their supporting pylons, a superstructure, hangers and columns.

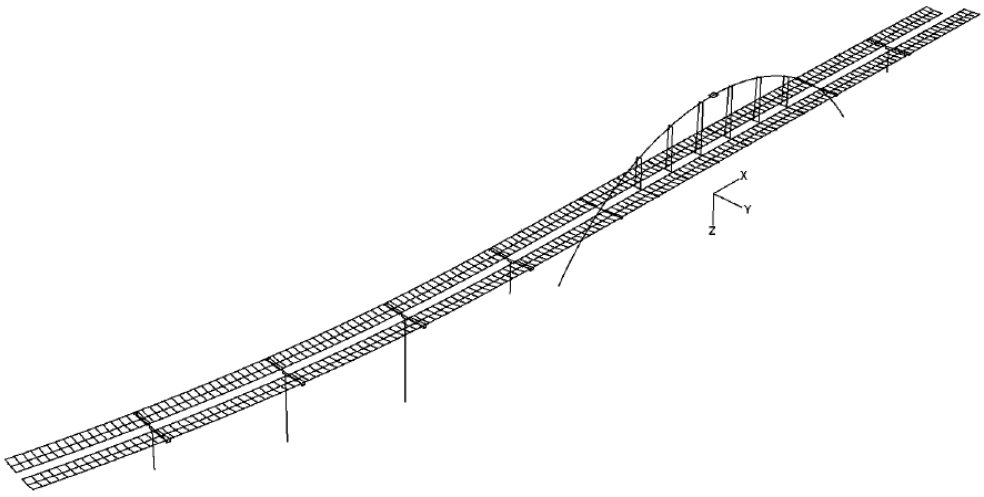

Figure 4.1 Finite element model of the New Svinesund Bridge from south-east, where all parts are visible except the temporary tendons and the supporting pylons.

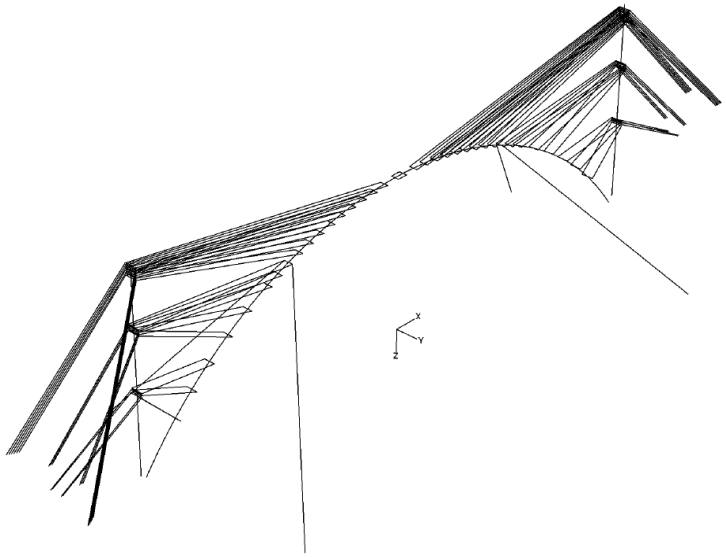

Figure 4.2 Finite element model of the arch and the temporary supporting structure with the steel bars visible in the arch crown.

4.1.2 Element types and properties

The FE-model of the bridge consists of three different element types, truss elements, beam elements and spring elements which are denoted in ABAQUS T3D2, B31 and SPRING1 respectively. Together with the specification of element type each element was given cross-sectional and material properties.

4.1.2.1 Truss elements

The T3D2 is a two node truss element in space with three active degrees of freedom, and can only transmit axial forces. This type of element was used to model the temporary tendons, and where each element was modelled as a SOLID SECTION. The sections were given a constant cross-sectional area and linear elastic material properties defined according to Bilfinger Berger (2004).

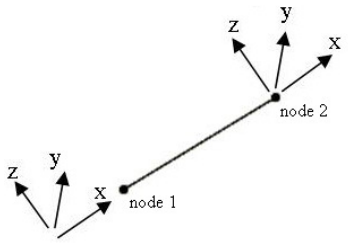

Figure 4.3 Principle figure of the truss element with its three active degrees of freedom.

4.1.2.2 Beam elements

The beam element B31 is a two node beam element in space with six active degrees of freedom. The beam element is based on Timoshenko beam theory that accounts for shear deformations. The elements have linear interpolation functions, and gives constant sectional forces along the element. All parts of the bridge, except the tendons, consist of this type of beam element but with different sectional and material properties.

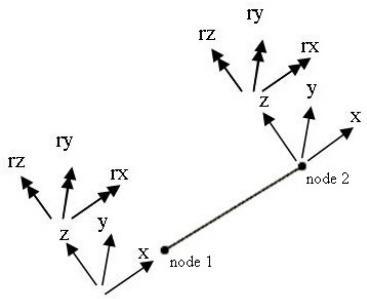

Figure 4.4 Principle figure of the beam element with its six active degrees of freedom.

The arch and the supporting pylons were modelled with hollow box cross-sections. Linear elastic material properties were used for the arch in the model including shrinkage while the material was modelled as viscoelastic in the creep model. The material of the supporting pylons was in both models modelled as linear elastic.

Other structural parts such as the carriageway, hangers, columns and the steel bars in the arch crown were modelled with a GENERAL beam section. This means that the cross sectional properties, such as cross-sectional area, moments of inertia and torsional rigidity are given explicitly together with Young's modulus and the shear modulus. In the model all these parts were modelled with linear elastic material properties. The carriageways were modelled as a beam grid structure to represent the box sections. Longitudinal beams were used to represent the longitudinal walls, and transversal beams representing the internal transversal stiffening walls of the bridge. Over each support and at the hangers, the two parallel carriageways are connected to each other with transversal beam elements. Both the hangers and the steel bars are modelled with beam elements given a very low bending stiffness, resulting in that they only transmit axial forces. The columns supporting the carriageways were modelled with beam elements located along the neutral axis of the columns.

The arch and the temporary pylons are modelled with beam elements positioned along their neutral axis. To be able to connect the tendons to the arch and pylons at the geometrically correct position in the section, stiff auxiliary cross beams were used as connectors.

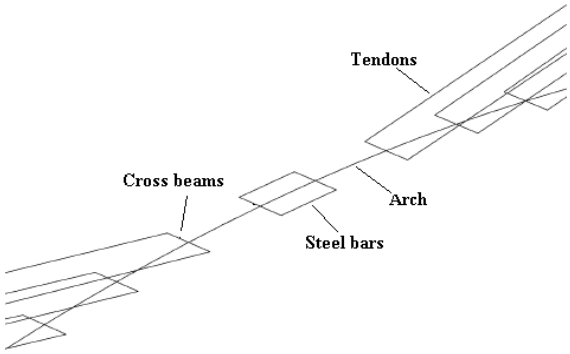

Figure 4.5 Figure showing how the auxiliary cross beams are used to connect the tendons and the steel bars to the arch.

4.1.2.3 Spring elements

SPRING1 is a spring element with translational and rotational degrees of freedom. The element only has one node free for displacement, while the other node is attached to the ground acting in the fixed direction.

Figure 4.6 Spring element with one fixed and one free node.

The spring element is used to model the support stiffness for the columns and the arch, in cases where it is not modelled as fixed or free. For each spring, the degree of freedom is given together with the corresponding linear translational or rotational stiffness, given from the Bilfinger Berger model (2004).

4.1.3 Boundary conditions

Concerning the boundary conditions the following assumptions were made according to Plos, Movaffaghi (2004):

- The arch was assumed to have fixed foundation for all degrees of freedom except the rotational around the bridge transverse axis. This degree of freedom was modelled by rotational springs, where the stiffness of the springs was taken from Bilfinger Berger (2003).
- The columns founded on rock (see Figure 2.1) were assumed to have fixed foundation for all translations and for torsion around the column axis. The support rotations around the bridge transverse and longitudinal axis were modelled by rotational springs. The stiffnesses given in the indata files from Bilfinger Berger (2004) were used. The rotational stiffness around the transverse axis corresponds to calculated stiffnesses in Bilfinger Berger (2003). The stiffnesses around the longitudinal axis were estimated to be about ten times greater.
- The column supported on piles (see Figure 2.1) was modelled with translational and rotational springs for all degrees of freedom. The stiffnesses of these springs where also taken from Bilfinger Berger (2003).
- The foundation of the supporting pylons and the rock anchor supports for the temporary tendons, were assumed to have all degree of freedom fixed.
- At the end abutments, on both the Swedish and Norwegian side, each carriageway was supported by two bearings. The support nodes closest to the centre-line of the bridge were fixed for both vertical and transversal displacement, while the other support nodes were fixed only in the vertical direction.

4.1.4 Loads

The response of the bridge was analysed with gravity and temperature loads. The density of the concrete was assumed to be 2500 kg/m^3 and the density of the steel to be 7850 kg/m^3. Concerning the density of the carriageways the steel density was modified to account for the additional weight of the asphalt layer. Measured values of the real hanger loads, see Jonsson, Johnson (2007), were compared to hanger loads from the model and a magnification factor was calculated.

4.1.5 Modelling of the construction process

When modelling the construction process of the bridge, the launching procedure was divided into several steps, where each step represented one or several construction events.

In the first analysis step all elements where removed from the model, and in the following steps a new part of the bridge were added to the analysis. After each event the shrinkage and the creep procedures were activated until the next event occurred.

During the construction of the arch, the prestressing level and the amount of strands in the temporary tendons varied. To be able to vary the amount of strands or the prestressing level at different stages in the analysis, each tendon was modelled with a number of parallel truss elements with different cross-sectional areas. When the prestressing level or the amount of strands were changed in the tendons, the current element was replaced with a new element with the correct cross-sectional area and a new prestressing level as initial stress.

When the arch launching was completed, the temporary supporting structure was removed and the remaining parts of the bridge were activated.

Below the principle analysis procedures for adding new parts and tendon modifications are described. This procedure was repeated until all parts of the bridge were added to the analysis.

- New parts

  Step 1- Activating of the element

  Step 2- Loading with self weight

  Step 3- Creep/Shrinkage until the next event

- Tendons

  Step 1- Activating and/or removing of strand elements

  Step 2- Loading with self weight

  Step 3- Creep/Shrinkage until the next event

5 Evaluation models

To be able to evaluate the effect of the sectional forces in the arch crown segment obtained from the structural FE-model of the bridge, two additional models were developed. One of these was a sectional model to investigate the response of the reinforced concrete section. The other was a local model of the attachment area of the steel bars to study the effect of the concentrated forces. These sectional and local models are described further in section 5.1 and 5.2 respectively.

5.1 Sectional model

The sectional response of the reinforced crown segment was studied for the combined action of normal force and bending moment. For this study a Matlab program that calculates the stresses and strains over the section due to the applied sectional forces developed by Schlune (2009), was used. This program was modified concerning geometry of the cross-section, time dependent material properties and loads. The hollow box-section of the crown segment was also simplified into an I-section (Figure 5.1) since the bending moments only act around the transverse axis.

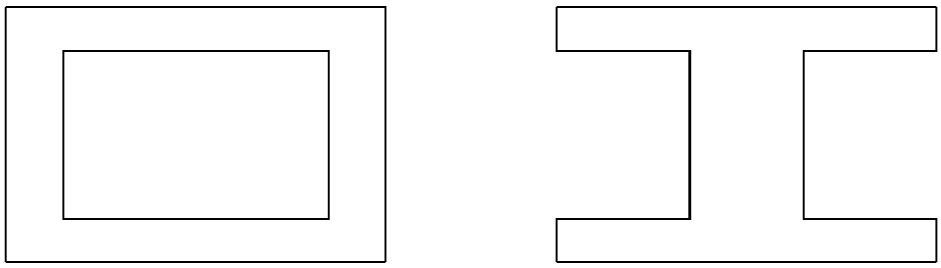

Figure 5.1 The original box-section and the simplified I-section.

The program calculated the stresses and strains through an iterative process shown in (Figure 5.2).

1. The section was discretized (Figure 5.3) and an initial men strain($\varepsilon_{initial}$) due to the normal force and a curvature($\kappa_{initial}$) due to the bending moment was assumed.
2. From the initial guess a total strain variation(ε_{tot}) over the section was calculated.
3. From the strain variation and the implemented material models (Figure 5.4) the corresponding reinforcement stresses(σ_s) and concrete stresses(σ_c)were found.
4. By a numerical integration of the stresses over the discretized section the corresponding sectional forces(SF_{num}) were calculated.
5. If the numerical sectional forces, SF_{num} , differed more than a certain tolerance from the applied sectional forces(SF) , a new updated strain(ε_{update}) and curvature(κ_{update}) was calculated using the Gauss-Newton algorithm and the procedure was then repeated.

6. When the required tolerance was fulfilled, the stress *($\sigma_{solution}$)* and strain *($\varepsilon_{solution}$)* variation over the section corresponding to the applied sectional forces, *(SF)*, has been found.

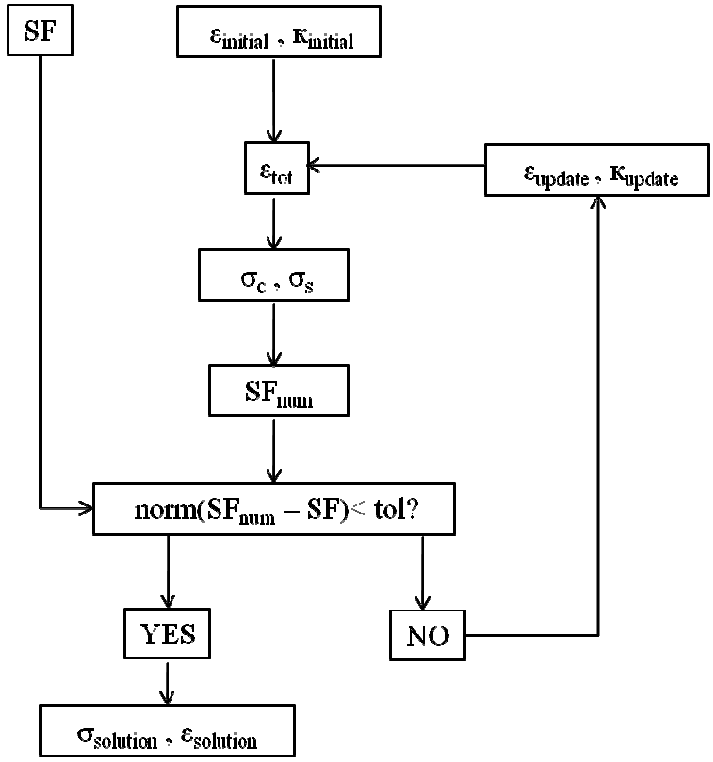

Figure 5.2 Flowchart of the program routine.

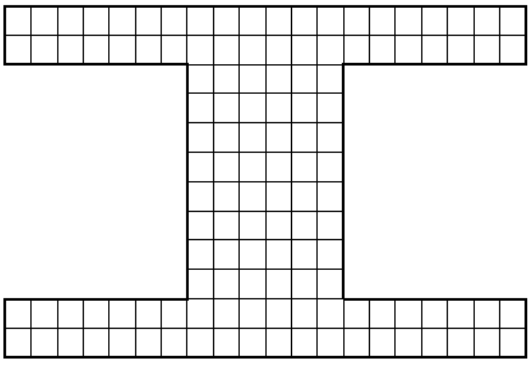

Figure 5.3 The principle of the discretized cross-section.

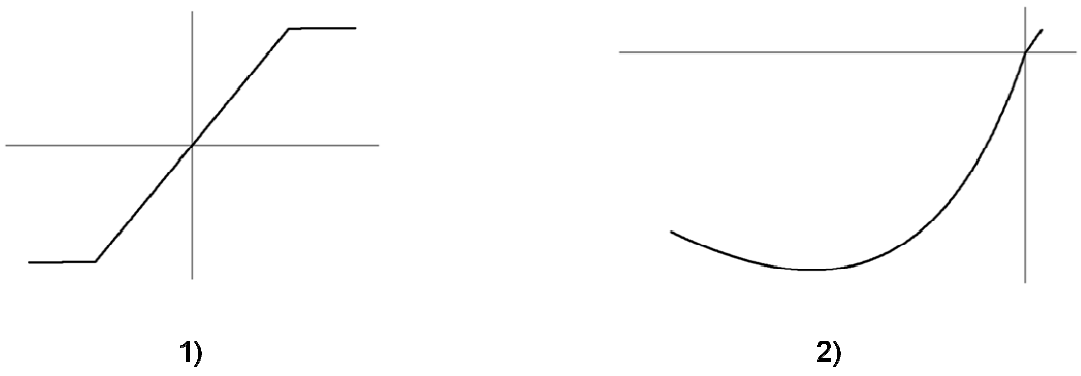

Figure 5.4 *1) Material model used for the reinforcing steel. 2) Material model used for the concrete. (EuroCode 2)*

5.2 Local model

To investigate if any risk of crushing or splitting are apparent in the attachment area of the steel bars, a local FE-model of this particular part was created in ABAQUS. A linear elastic analysis was performed to identify areas with high stresses and to evaluate if the magnitude of these stresses are such that a risk of cracking or splitting exist.

The model was simplified and approximated into a two dimensional problem (Figure 5.5) by dividing the segment at the vertical symmetry line of the cross-section, and by assuming that the loading plate was acting over the full width of the web. To include the stiffness contribution from the flanges, these areas were given a thickness corresponding to the width of the flanges.

The length of the part included in the model was taken as the length of the segment approximated to be twice the height of the section, i.e. the disturbed region in which the concentrated stresses are assumed to distribute, Engström (2006).

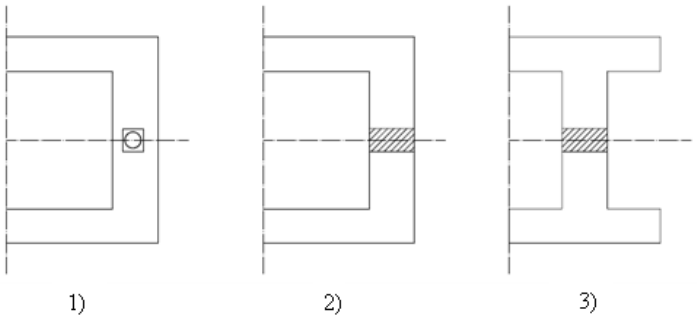

Figure 5.5 *1) Section divided by a vertical symmetry line, 2) extension of the loading plate over the width of the web, 3) approximation of the position of the web.*

5.2.1 Element types and properties

The elements used for the model were two-dimensional, plane stress continuum elements. The elements were four-node bilinear, elements called CPS4R in ABAQUS. All parts, the web, the flanges and the loading plate were assigned a thickness corresponding to the real geometry according to Figure 5.6. The web and flanges were given material properties of concrete, while the loading plate was given fictitious material properties with large stiffness.

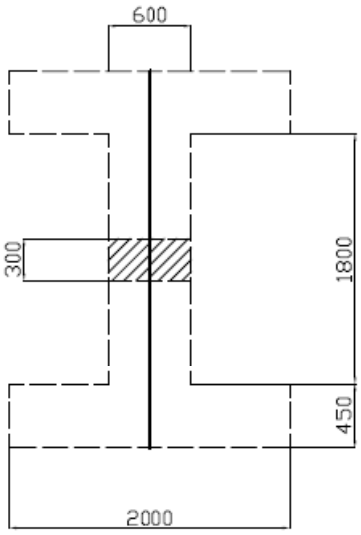

Figure 5.6 Geometry of the modelled section with the plane stress elements positioned in the symmetry line.

5.2.2 Loads and Boundary conditions

The sectional forces in the steel bars from the global structural model were used as force input in this model. Since the force varies with time several magnitudes of the load was considered. The force was transformed to a pressure load acting on the boundary of the loading plate.

The boundary conditions of the model were assumed to be fully fixed at the boundary towards the adjacent segment.

Figure 5.7 View of the segment with the loading plate to the left and a fixed boundary to the right.

6 Analysis results

From the global structural analysis of the bridge, the sectional forces in the arch crown were studied. The analyses were performed to reflect the entire service life of the bridge and a special interest has been to study how the sectional forces vary with time in the arch crown. The results obtained from the structural analysis were used in a sectional analysis to evaluate the response of the crown segment, and in a local analysis of the attachment area of the steel bars to investigate the risk of concrete crushing or splitting.

6.1 Structural model

The structural analysis was performed with influence of creep, shrinkage and temperature variations. The forces in the arch crown were studied from the day of installation of the steel bars until 120 years after the bridge was completed. Since two types of structural models were used to be able to reflect the influence of the long-term effects and temperatures, the results from the analyses were superimposed.

In Figure 6.1 to Figure 6.3 the development over time of the sectional forces for the arch crown segment and the steel bars are presented. By studying the entire time-span it can be seen that the magnitude of the normal force in the steel bars (Figure 6.1) increases with time, while the forces in the crown segment (Figure 6.2) are decreasing. This behaviour was expected since a redistribution of forces occurs from the concrete in the segment to the bars due to the long-term effects. The bending moment (Figure 6.3) has its maximum values early in the time-span, namely during the construction of the bridge.

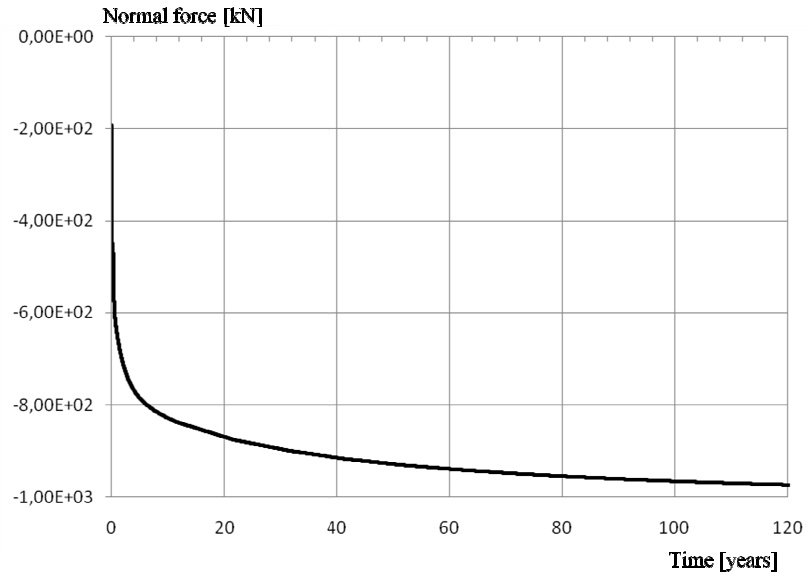

Figure 6.1 Variation of normal force in each of the steel bars during the service life of the bridge. The normal force is influenced by both creep and shrinkage.

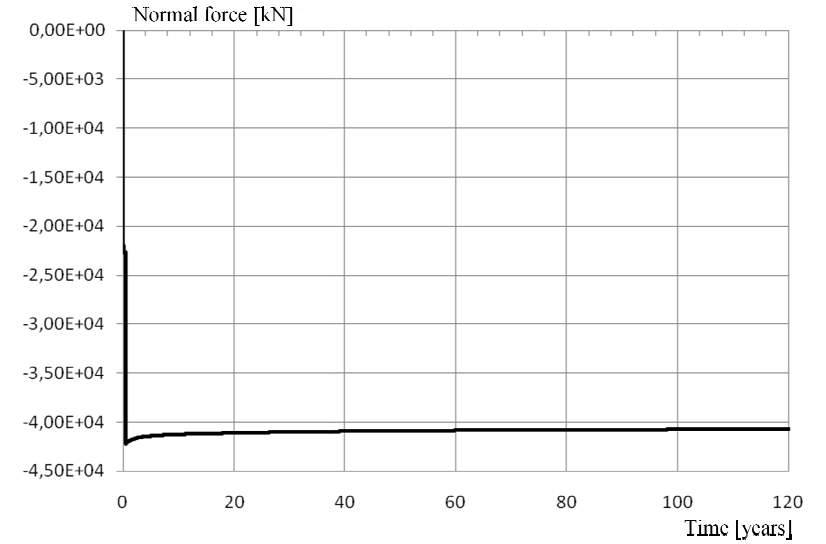

Figure 6.2 Variation of normal force in the crown segment during the service life of the bridge. The normal force is influenced by both creep and shrinkage.

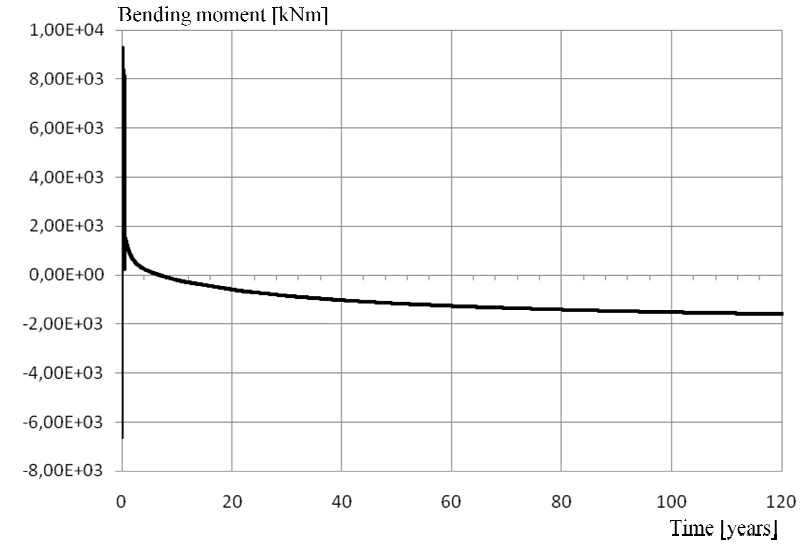

Figure 6.3 Variation of moment in the crown segment during the service life of the bridge. The moment is influenced by both creep and shrinkage.

From the results discussed concerning the sectional moments in the crown segment a study was performed of the force distribution during the construction of the bridge. The events that were considered to be of interest to study during the construction are presented in Figure 6.4. In Figure 6.5 to Figure 6.7 the sectional forces from the construction phase are shown together with the interesting events. In Appendix H the distribution of the sectional forces and moments over the entire arch is presented together with the above mentioned stages.

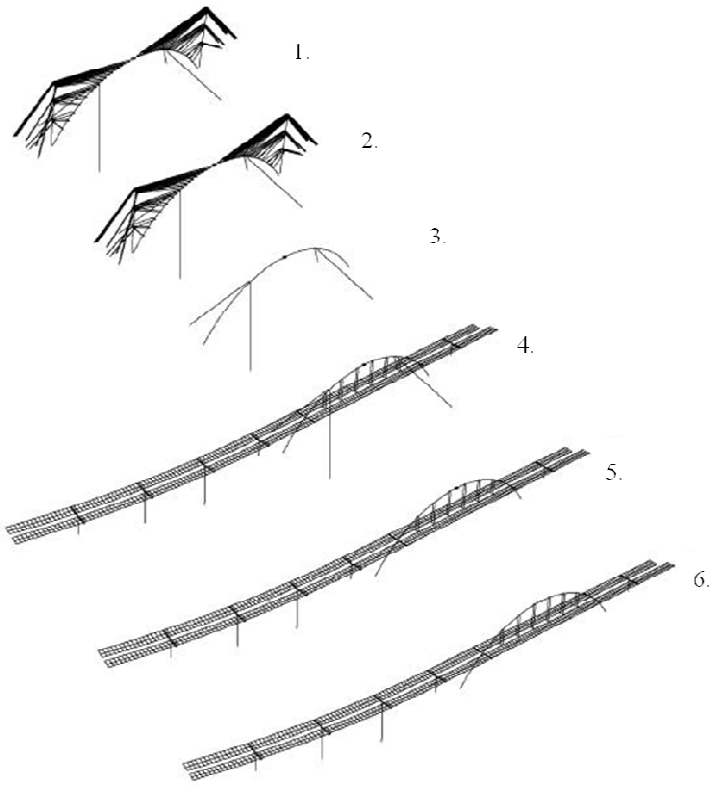

Figure 6.4 *1. Installation of the steel bars*
2. After casting of the crown segment
3. After removal of the temporary supporting structures
4. Completed bridge before removal of the lateral supporting tendons
5. Completed bridge
6. End of service life after 120 years

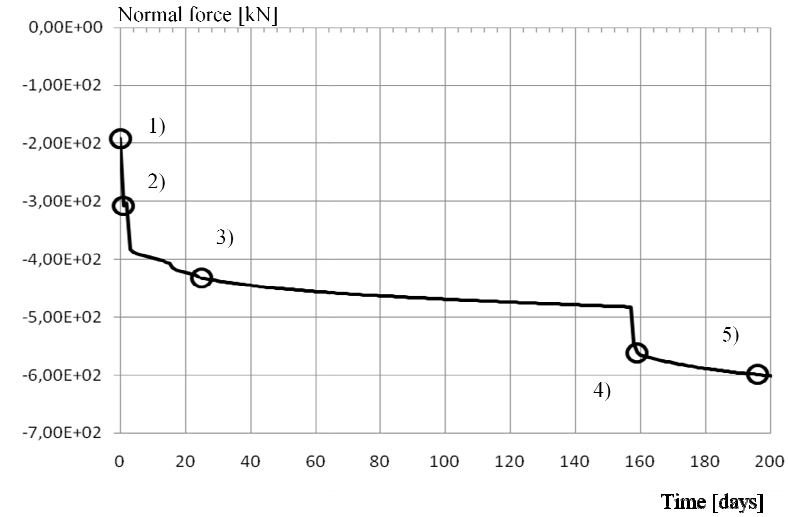

Figure 6.5 Normal force distribution in each bar during the construction phase.

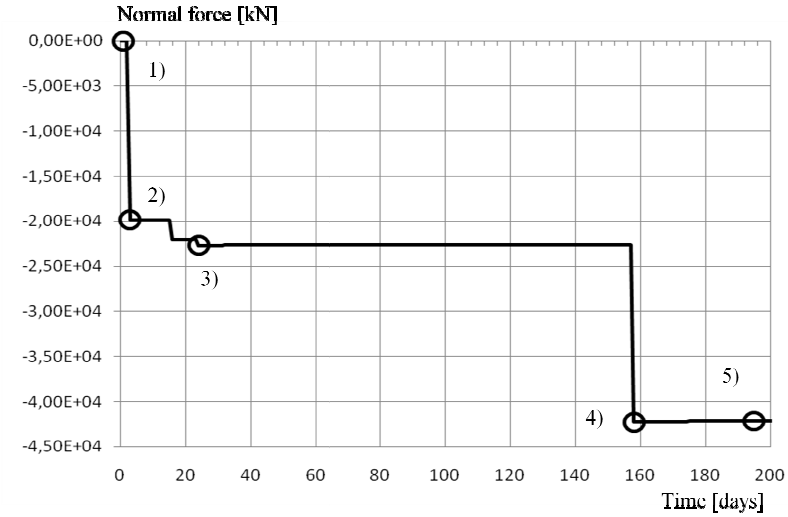

Figure 6.6 Normal force distribution in crown segment during the construction phase.

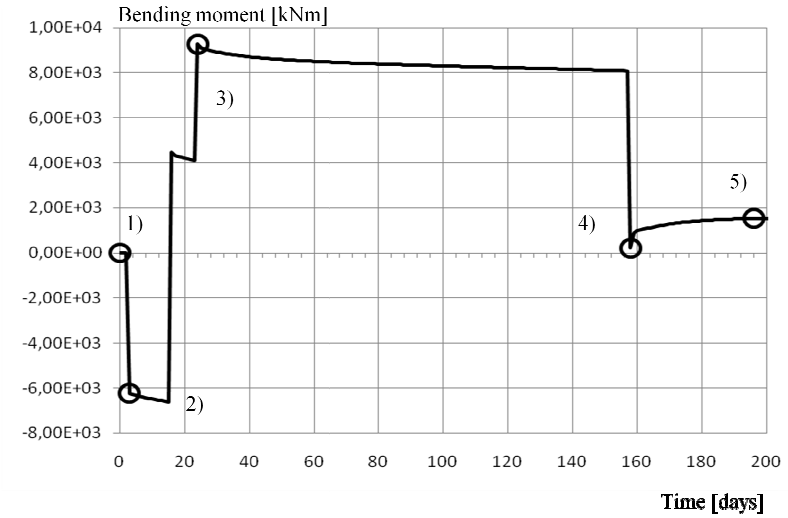

Figure 6.7 Bending moment distribution in the crown segment during the construction phase.

From the results presented it can be seen that the construction phase of the bridge has a great influence on the sectional forces and the moments in the crown segment. A combination of high bending moments and low normal forces could be critical in the sense that some parts of the section might be subjected to tensile forces. In the long-time perspective on the other hand, the moments are very small in combination with high normal forces which are more favourable to maintain the entire section in a compressed state. Regarding the normal force in the steel bars the force is increasing with time and reaching its maximum value in the end of the time-span, leading to an increase of stresses in the attachment area throughout the service life of the bridge.

6.1.1 Influence of long-term effects

In Figure 6.8 to Figure 6.9, the influence of the long-term effects is compared to the static case without the influence of creep and shrinkage. It can be seen that the long-term effects have the largest influence on the bending moment in the crown segment (Figure 6.8) and on the normal force in the steel bars (Figure 6.9), while the influence on the normal force in the crown segment (Figure 6.10) is not as apparent as the previous mentioned.

During the service life the long-term effects has a favourable effect on the sectional response of the crown segment. This is concluded since the bending moment is greatly reduced compared to the static case, while the normal force in the segment is almost unchanged. Concerning the concentrated forces in the attachment area of the steel the long-term effects have an unfavourable effect due to the increasing normal forces in the bars.

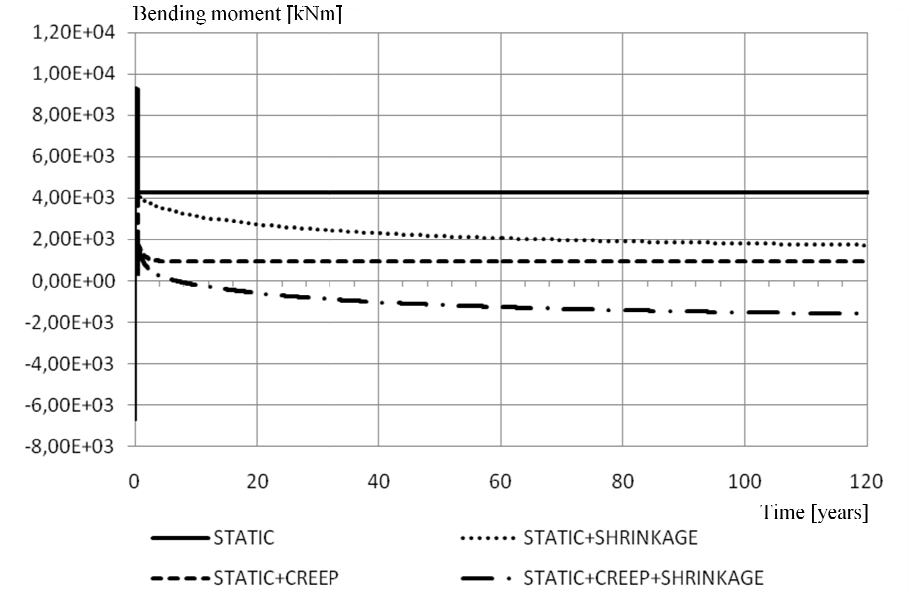

Figure 6.8 Comparison of the moment variation in the crown segment influenced by creep and shrinkage.

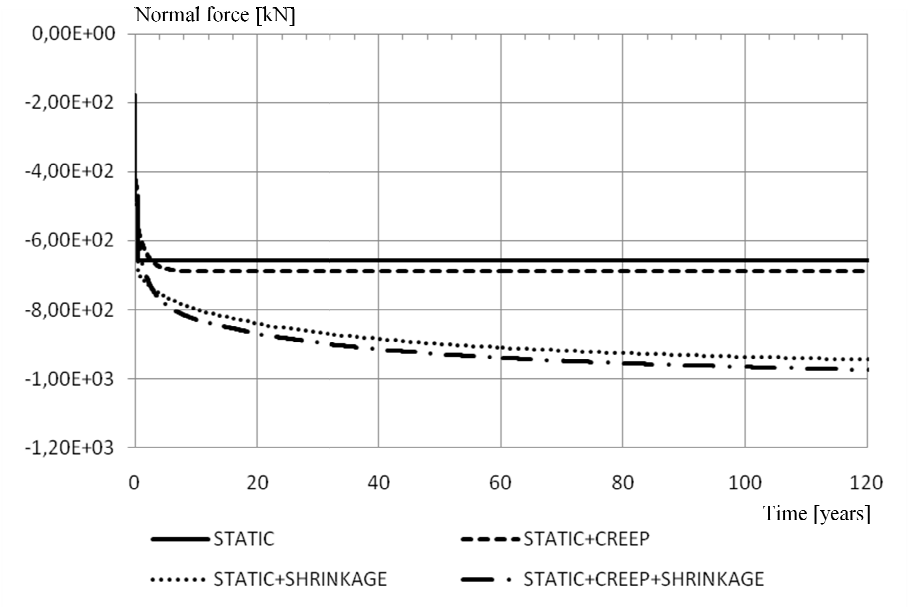

Figure 6.9 Comparison of the normal force variation in each steel bar influenced by creep and shrinkage.

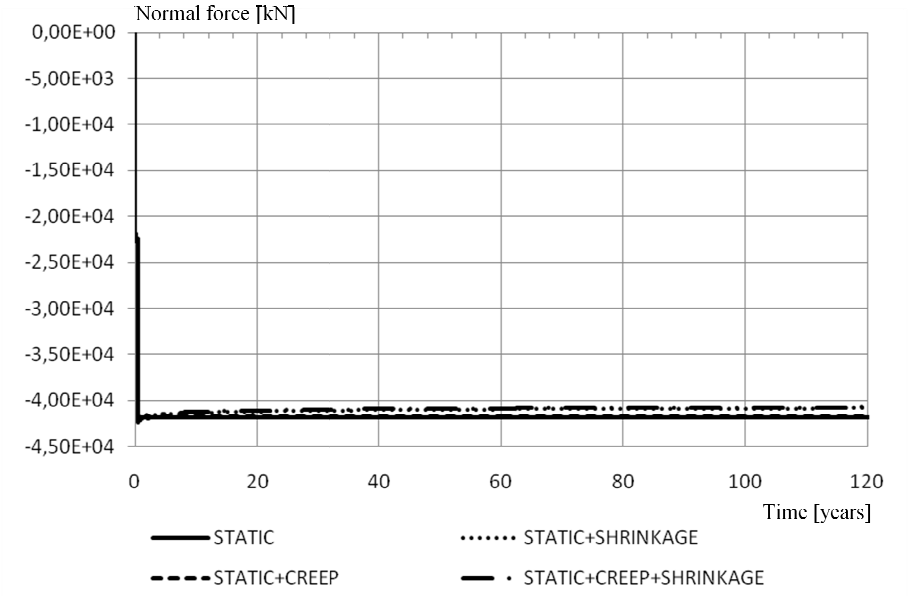

Figure 6.10 Comparison of the normal force variation in the crown segment influenced by creep and shrinkage.

6.1.2 Influence of temperature

In Figure 6.11 Moment variation over time in the crown segment influenced of creep, shrinkage and temperature. In Figure 6.11 to Figure 6.13, the results from the analysis including temperature variations are compared to the analysis including creep and shrinkage. Due to the linear elastic model the sectional forces will vary linearly with the temperature. Therefore the temperatures were chosen to $\Delta T=30^{o}C$ and $\Delta T=-30^{o}C$ to find the relation between the sectional forces and the temperature. By interpolation it was then possible to study the effects of different temperatures acting on the structure. The results shows that a positive temperature is more unfavourable for the crown segment since the bending moment (Figure 6.11) increases and the normal force (Figure 6.13) is decreasing. The normal forces in the steel bars (Figure 6.13) are also increasing and thus the stresses in the attachment area.

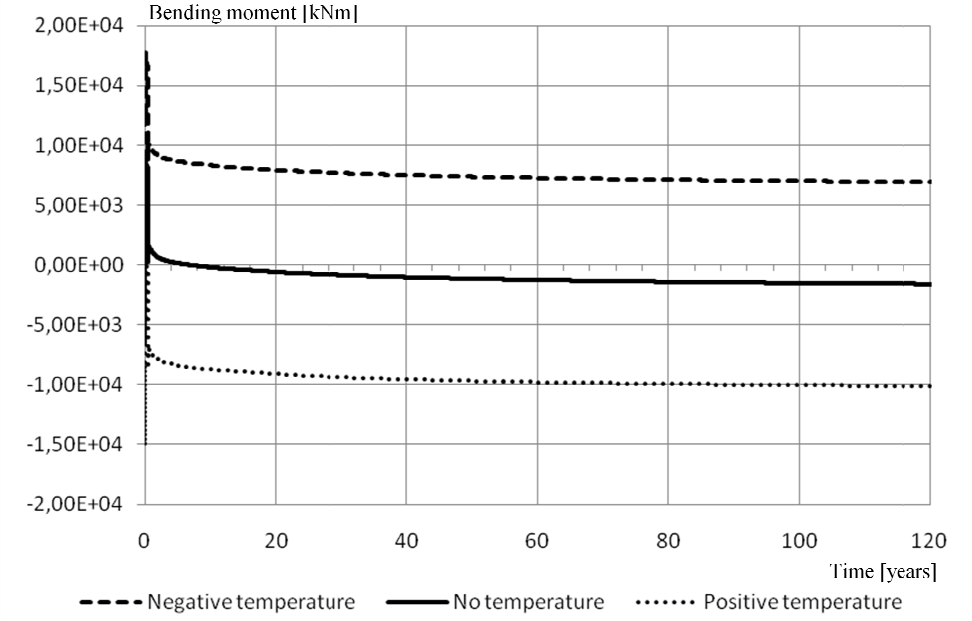

Figure 6.11 Moment variation over time in the crown segment influenced of creep, shrinkage and temperature.

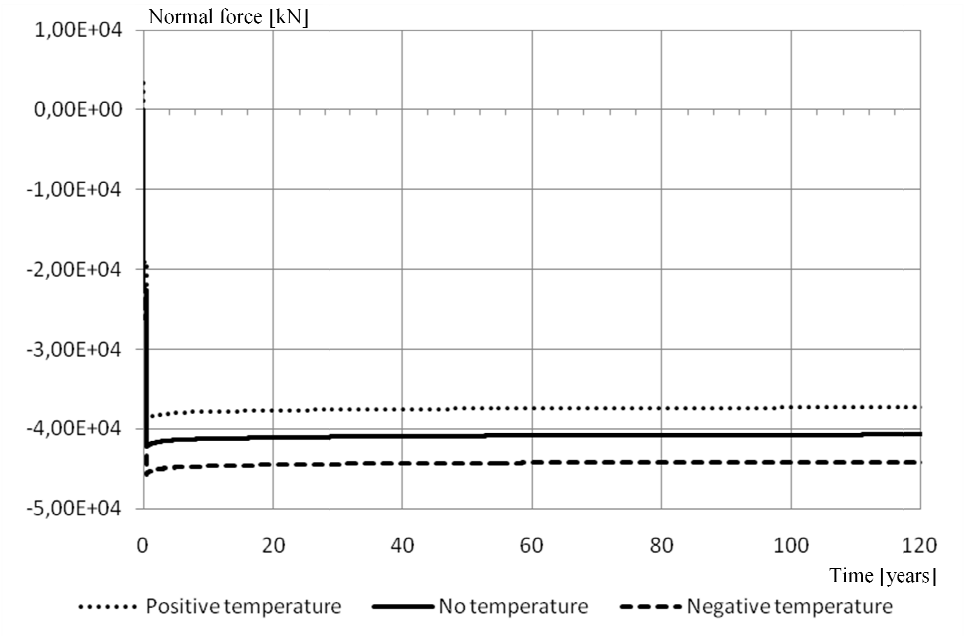

Figure 6.12 Normal force variation with time in the top segment influenced of creep, shrinkage and temperature.

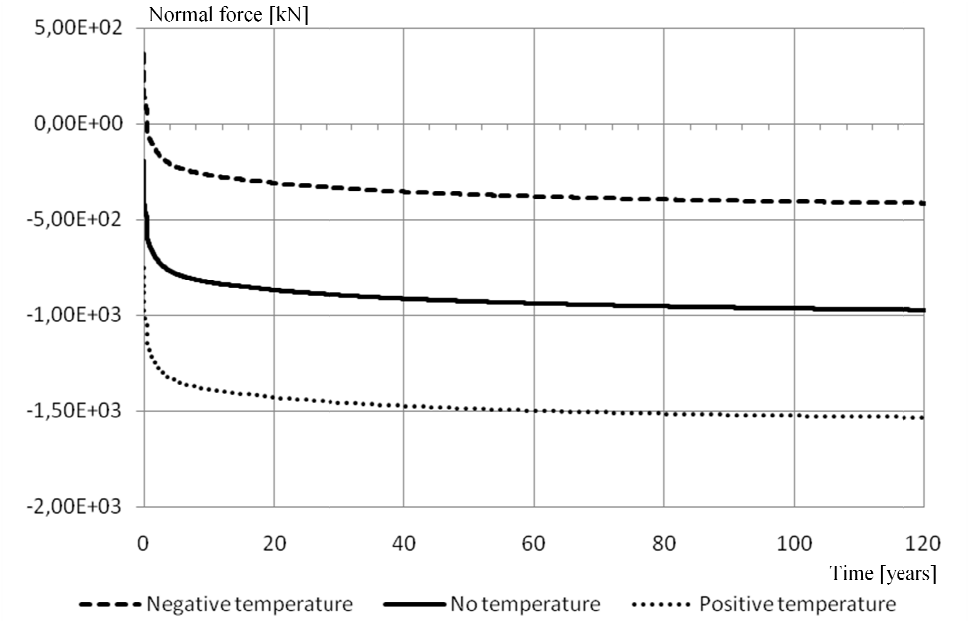

Figure 6.13 Normal force variation with time in each bar influenced of creep, shrinkage and temperature.

6.2 Sectional model

With the Matlab program created for the sectional analysis the stresses where calculated. The analysis of the sectional response was performed during the construction phase due to the unfavourable conditions with large bending moments and relatively small normal forces.

In Figure 6.14 the stresses in the outer most fibres are plotted together with the resistance of the section. It can be seen that the section always remains in a compressed state. It can also be seen that the stresses over the section becomes more or less constant after the installation of the carriageways (stage 4).

The effect of the ambient temperature has also been controlled by implementing the daily mean temperature documented from the actual construction of the bridge. The results from the analysis are shown in Figure 6.15 and the stresses influenced by temperature do not differ significantly from the case without influence of temperature.

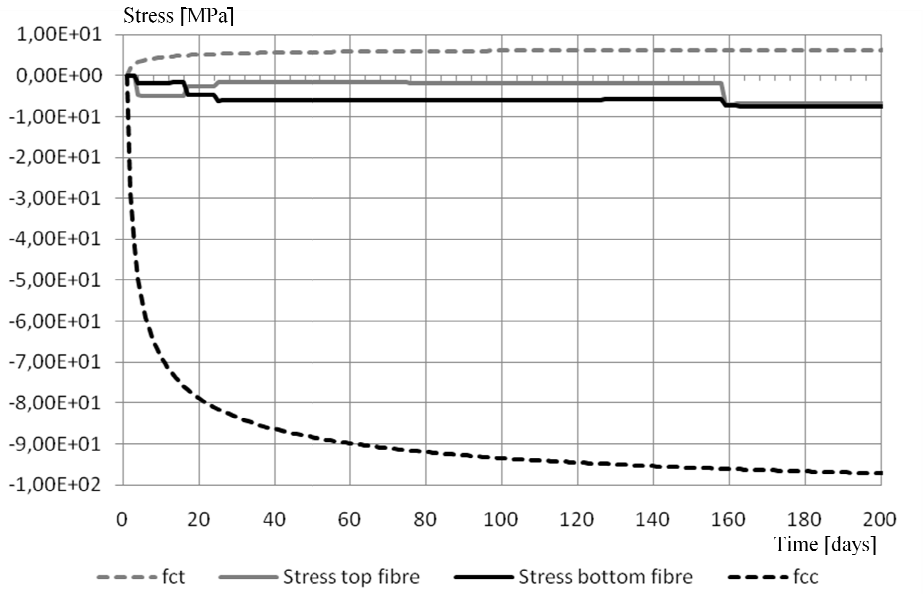

Figure 6.14 Stress compared to the resistance of the concrete.

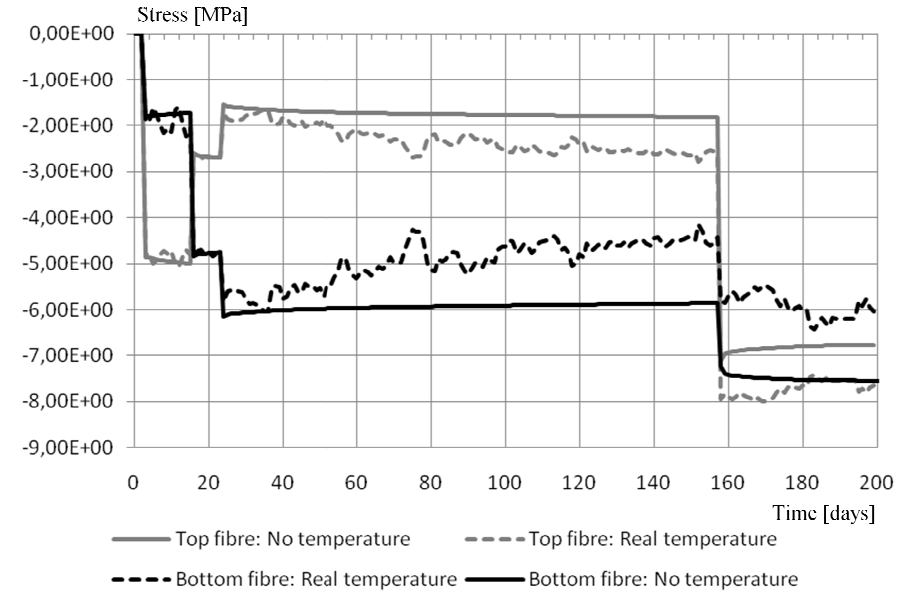

Figure 6.15 Stresses in the outer most fibres for the cases with measured temperature and no temperatures.

6.3 Local model

The investigation concerning crushing or splitting in the attachment area of the steel bars have been controlled construction stages 1 to 5 and at the end of the service life of the bridge (stage 6). These forces and the corresponding concrete properties were implemented in the local FE-model. Two analyses were performed, one including creep and shrinkage while the second also included a large positive temperature ($\Delta T=30^{o}C$). These results, presented in terms of principal stresses, are shown in Figure 6.16 and Figure 6.17 together with the resistance of the material. In both cases the principal stresses are shown to be well below the resistance, and therefore no crushing or splitting of the disturbed region is expected to occur.

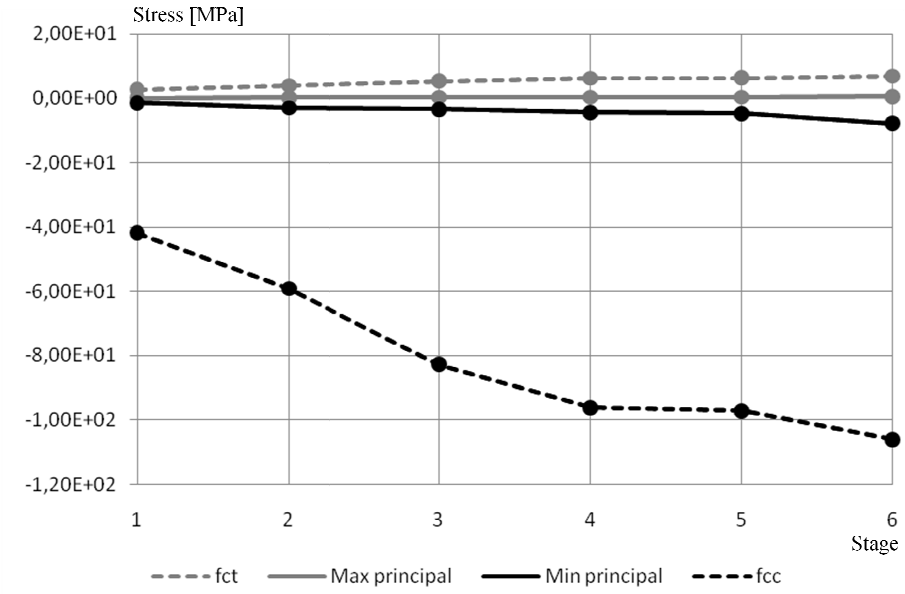

Figure 6.16 The principal stresses compared to the resistance of the material, based on the results from the analysis only including creep and shrinkage.

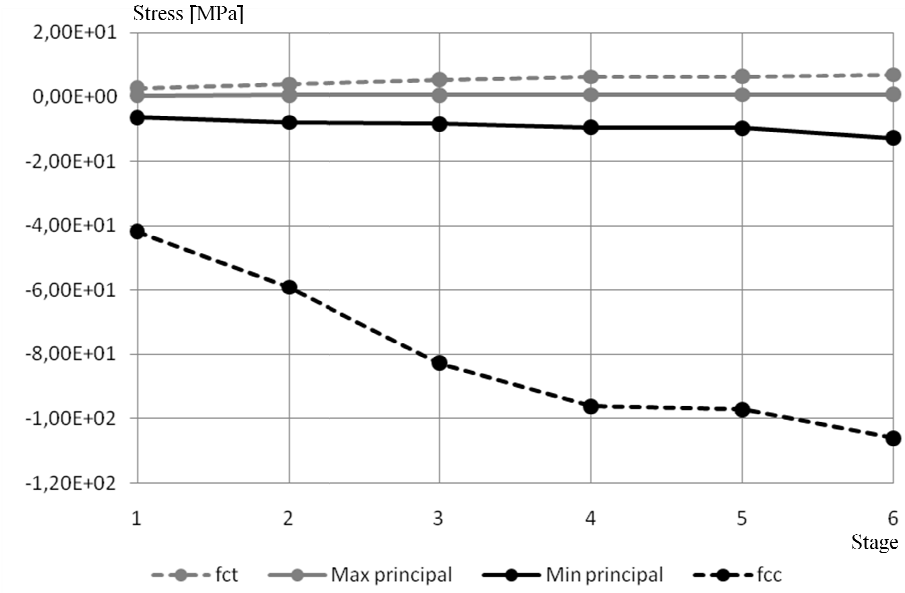

Figure 6.17 The principal stresses compared to the resistance of the material, based on the results from the analysis including creep, shrinkage and a positive temperature.

7 Conclusions

In thesis the following was achieved:

- The finite element model of the New Svinesund Bridge has been furthered developed by a more accurate analysis of the arch launching. The input data for the modelling of the arch launching was taken from documented data from the real events when constructing the arch, where the main focus was on the events during the closing of the arch halves.
- Each segment of the arch has been modelled with individual material parameters based on documented strength test data, and geometrical conditions based on construction drawings.
- The option *SWELLING was implemented in the material model to describe the shrinkage behaviour of concrete, where this option defines a time dependent volumetric swelling of the material.
- The viscoelastic material model describing creep, developed by Canovic, Goncalves (2005) was updated with a more accurate input data consisting of smaller time steps over a longer time period.
- The analysis was improved to analyse the structural behaviour during the entire service life of the bridge, i.e. 120 years.
- An improved analysis of the arch crown connection was performed by two local models of this particular area. A model to analyse the sectional response from the combined action of bending moment and normal force was created, together with a model to analyse the disturbed regions of the attachment area of the steel bars was created.

The following conclusions can be drawn based on the results obtained from the analyses:

- The influence of creep and shrinkage has a more favorable effect on the sectional response of the arch crown in the long time perspective compared to the static case. This is due to the fact that the bending moments are reduced while normal force in the crown segment is in practical unchanged i.e. the section will be in a more uniform compressed state. The critical events concerning the sectional response was found to occur during the construction of the arch where the structure were subjected to high bending moments and low normal force. The steel bars will carry an increasing part of the normal force over time due to the long-term effects.
- The influence of a positive temperature is more unfavorable for the crown segment since the bending moment increases and the normal force decreases with increasing temperature. The effect of a negative temperature on the other hand reduces the bending moment and increases the normal force in the crown segment. Concerning the normal force in the steel bars, the forces will increase with an increasing positive temperature.

- The cross-section of the arch crown remains in compression during the entire service life of the bridge. After long time the stresses over the section becomes more or less uniform. The principal stresses in the disturbed region are increasing with the increasing normal force in the steel bars. The magnitude of stresses over the section and the stresses in the disturbed regions are much smaller than the strength of the material. Therefore problems regarding the future performance of the arch crown are not likely.
- Modeling with individual material parameters of the arch segments does not have a significant influence on the response.

It should be noted that the results from the creep and the shrinkage analyses were superimposed. This assumption implies that shrinkage and the creep behave independently of each other, but this is not the case in reality. The shrinkage forces in the arch arise due to the restraint caused by the supports and the carriageways. This means that the shrinkage forces also will be effected by creep, or in this case relaxation, due to these hindrances. Therefore the influence of shrinkage will not be as pronounced as in the super imposed results.

The following conclusions can be drawn concerning the modeling process:

- The development of Young's modulus with time that was modeled by Canovic and Goncalves was found to not work as intended. This could depend on that the new version of ABAQUS, used in this thesis, might not support the option used in the old version.
- When defining the viscoelastic material to describe creep in the material specification, it is important to define a large amount of data points with small time steps. Since ABAQUS uses a least-square fit to solve the parameters in the Prony series expansion, the intended creep function might not be as desired when too few data points are used. It is also important to insert data points that more or less follow a curve similar to an exponential function otherwise ABAQUS will have a problem performing the least square fit.
- The material model that was used in this thesis to describe shrinkage cannot be combined with the viscoelastic material model that included creep, developed by Canovic and Goncalves (2005). However in the late stages of this project an option using the subroutine CREEP was found. In this option a viscoelastic material is defined by a Prony series expansion, describing a time dependent volumetric change of a material. Since this option is based on the same subroutine as the material model developed by Canovic and Goncalves, there could be a possibility to combine these two material models.

Other possible improvements of the FE-model and the evaluation of the bridge:

- To model the arch and the carriageways with different temperature gradients over the sections. Since the concrete arch is denser than the steel carriageways, it would not respond in the same way with temperature changes.
- Study aerodynamic structural response of the bridge by modelling wind actions on the bridge.
- Study the structural behaviour of the bridge due to the combined action of traffic-, wind- and temperature loads on the bridge.

8 References

Bazant and Wittmann. (1982). *Creep and shrinkage in Concrete Structures.* New York: Jhon Wiley & sons.

Bilfinger Berger. (2003a). *"14-1319-1 BRO ÖVER IDEFJORDEN (NY SVINESUNDSBRO) VID BJÄLLVARPET Å VÄG E6, plan och sectioner" 113k2005.* Vägverket, Region Väst.

Bilfinger Berger. (2004). *Indata files for the structural model of the New Svinesund Bridge.* Mannheim, Germany: Bilfinger Berger.

Bilfinger Berger. (2003b). *Launching of the arch (Document no. 116K1305, 116K1317, 116K1333).* Mannheim, Germany: Bilfinger Berger.

Canovic and Goncalves. (2005). *Modelling of the response of the New Svinesund Bridge - FE Analysis of the arch launching.* Göteborg: Department of Civil and Environmental Engineering.

CEN. (2002). *Eurocode 2: Designe of concrete structures - part 1-1: General rules and rules for buildings.* Brussels: European Standard.

Comite' Euro-International du Béton. (1993). *CEB FIP Model-code 1990.* Lausanne: Thomas Telford Service Ltd.

Darholm, Lundh, Ronnebrandt, Karoumi and Blaschko. (2007). *Svinesundsbron Teknik & utförande.* Uddevalla: Vägverket.

Domone and Illston. (2008). *Construction materials and their behaivour and nature.* New York: Spon press.

Engström. (2006). *Design and analysis of deep beams and othe discontinuity regions.* Göteborg: Department of Civil and Environmental Engineering Chalmers University of Technology.

Fédération internationale du Béton. (2009). *Structural concrete textbook on behaviour, design and performance.* Lausanne: Document Competence Center Siegmar Kästl e.K.

Hibbit, K. a. (2002). *ABAQUS/Standard Version 6.3 Manual theory and Kewords Manual.* USA: Hibbit, Karlson and Sorensen Inc.

James and Karoumi. (2003). *Monitoring of the New Svinesund Bridge - Instrumentation of the arch and preliminary results from the construction phase.* Stockholm: Department of Civil and Architectural Engineering, KTH.

James and Karoumi. (2004). *Monitoring of the New Svinesund Bridge - Presentation of some measured data including the lifting of the mid-section of the bridge deck on 25 July.* Stockholm: Department of Civil and Architectural Engineering, KTH.

Jonsson and Johnson. (2007). *Finite Element Model Updating of the New Svinesund Bridge - Manual Model Refinement with Non-Linear Optimization.* Göteborg: Department of Civil And Environmental Engineering.

Movaffaghi and Plos. (2004). *Finite Element Analysis of the New Svinesund Bridge - Design model conversion and analysis of the arch launching.* Göteborg: Department of Structural Engineering and Mechanics, Chalmers University of Technology.

Schlune. (2009). *Improvmed Bridge Evaluation.* Göteborg: Department of Civil and Environmental Engineering, Chalmers University of Technology.

Appendix A

```
%%%%%%%%%%%%%%%%%%%%%%%%%%%%%%%%%%%%%%%%%%%%%%%%%%%%%%%%%%%%%%%%%%%%%%%%%%%%
%
% Calculation of the increase of concrete
% material properties with time
%
% Calculations are based on time-functions from
% CEB-FIB Model Code 1990
%
% Per Lindberg & Jonas Nilsson                          2010-04-26
%
%%%%%%%%%%%%%%%%%%%%%%%%%%%%%%%%%%%%%%%%%%%%%%%%%%%%%%%%%%%%%%%%%%%%%%%%%%%%

%-------------------- Mean compressive strength ---------------------

[fcm]=Strength(0);                          %[Pa] Strength test data

%-------------------------- Time-function ---------------------------

%%betacct=exp(s*(1-sqrt(28/t))) = time function
%%t = age of concrete [days]
%%s = coefficient depending on type of cement (Class N)

s=0.25;
t=1:1:500;
betacct=exp(s*(1-sqrt(28./(t))));                                Eq 2.1-54

%-------------------- Compressive strength growth -------------------

fcmt=(betacct*fcm)*10^-6;                   %[MPa]           Eq 2.1-53

%-------------------- Growth of Young's modulus ---------------------

Ec0=2.15*10^10;                             %[Pa]
fcm0=10*10^6;                               %[Pa]
%%Coefficient which depends on the age of concrete
betaEt=sqrt(betacct);                                            Eq 2.1-58
%%Modulus of elasticity at concrete age of 28 days
Eci=Ec0*(fcm/fcm0)^(1/3);                   %[Pa]                Eq 2.1-16
%%Reduced modulus of elasticity for elastic analysis of concrete
structures
Ec=0.85*Eci;                                %[Pa]                Eq 2.1-17
%%Modulus of elasticity at an age t days
Ecit=betaEt*Ec*10^-9;                       %[GPa]               Eq 2.1-57

%------------------- Tensile strength growth ------------------------

fck=fcm-8*10^6;                             %[Pa]                Eq 2.1-1
fck0=10*10^6;                               %[Pa]
fctk0m=1.4*10^6;                            %[Pa]
fctm=fctk0m*((fck/fck0)^(2/3));             %[Pa]                Eq 2.1-4
fctmt=(betacct*fctm)*10^-6;                 %[MPa]
```

Appendix B

```
%%%%%%%%%%%%%%%%%%%%%%%%%%%%%%%%%%%%%%%%%%%%%%%%%%%%%%%%%%%%%%%%%%%%%%%%%%%%
%
% Calculating the development of shrinkage strain according to
% CEB-FIB Model Code 1990.
%
% To be implement these effects into Abaqus the shrinkage stain is
% transformed into an equivalent temperature acting on the concrete.
%
% Per Lindberg & Jonas Nilsson                          2010-04-26
%
%%%%%%%%%%%%%%%%%%%%%%%%%%%%%%%%%%%%%%%%%%%%%%%%%%%%%%%%%%%%%%%%%%%%%%%%%%%%

%----------------- Calculating the shrinkage strain -----------------

[fcm]=Strength(0)       %[Pa] Concrete strength based on test data
fcm0=10*10^6;           %[Pa]

t=0:1:43800;            %Age of concrete [days]
ts=0;                   %Age when shrinkage begins [days]
t1=1;                   %[day]

RH=75;                  %Relative humidity [%]
h0=0.100;               %[m]
RH0=100;                %[%]
betasc=5;               %for rapid and normal cement

[h]=notsize(0);         %notional size of the member. Eq 2.1-69

for i=1:length(t)
    betasdt=(((t(i)-ts)/t1)/((350*(h/h0)^2)+((t(i)-ts)/t1)))^0.5;
                                                          Eq 2.1-79
    betasRH=1-(RH/RH0)^3;                                 Eq 2.1-78
    betaRH=-1.55*betasRH;                                 Eq 2.1-77
    epssfcm=(160+ 10*betasc*(9-fcm/fcm0))*10^-6;          Eq 2.1-76
    epscs0=epssfcm*betaRH;                                Eq 2.1-75
    Epscs=epscs0*betasdt;                                 Eq 2.1-74
    eps(i)=Epscs;
end
```

Appendix C

```
%%%%%%%%%%%%%%%%%%%%%%%%%%%%%%%%%%%%%%%%%%%%%%%%%%%%%%%%%%%%%%%%%%%%%%%%%%%%
%
% Implementation of the material model describing shrinkage in ABAQUS
%
%%%%%%%%%%%%%%%%%%%%%%%%%%%%%%%%%%%%%%%%%%%%%%%%%%%%%%%%%%%%%%%%%%%%%%%%%%%%

*MATERIAL, NAME=SS0
*ELASTIC
41E9, 0.2
*SWELLING, DEPENDENCIES=1, LAW=INPUT
** Strain rate    ,   Temp    ,Field variable
-0.0000008023     ,     0     ,     1
-0.0000003697     ,     0     ,     2
-0.0000003407     ,     0     ,     3
-0.0000003115     ,     0     ,     4
-0.0000002723     ,     0     ,     5
-0.0000002507     ,     0     ,     6
-0.0000002394     ,     0     ,     7
-0.0000002281     ,     0     ,     8
-0.0000002169     ,     0     ,     9
-0.0000002112     ,     0     ,     10
-0.0000002044     ,     0     ,     11
-0.0000001947     ,     0     ,     12
-0.0000001871     ,     0     ,     13
-0.0000001822     ,     0     ,     14
-0.0000001784     ,     0     ,     15
-0.0000001742     ,     0     ,     16
-0.0000001687     ,     0     ,     17
-0.0000001625     ,     0     ,     18
-0.0000001584     ,     0     ,     19
-0.0000001556     ,     0     ,     20
...
```

Appendix D

```
%%%%%%%%%%%%%%%%%%%%%%%%%%%%%%%%%%%%%%%%%%%%%%%%%%%%%%%%%%%%%%%%%%%%%%%%%%%%
%
% Calculating the development of the creep coefficient according to
% CEB-FIB Model Code 1990.
%
%
% Per Lindberg & Jonas Nilsson                          2010-04-26
%
%%%%%%%%%%%%%%%%%%%%%%%%%%%%%%%%%%%%%%%%%%%%%%%%%%%%%%%%%%%%%%%%%%%%%%%%%%%%

t1=1;                   %[day]
RH0=100;                %[%]
h0=0.1;                 %[m]
fcm0=10;                %[MPa]

[fcm]=Strength(0);      %[Pa] Concrete strength based on test data
fcm=fcm*10^-6;          %Compressive strength of concrete [MPa]
t0=1;                   %Age of concrete when loaded [days]
t=1:10000;              %Time [days]
RH=75;                  %Relative humidity of the ambient environment
[h]=notsize(0);         %Notational size of the member [m]

for i=1:length(t)

BETAt0=1/(0.1+(t0/t1)^0.2);                             %Eq 2.1-68
BETAfcm=5.3/((fcm/fcm0)^0.5);                           %Eq 2.1-67
FiRH=1+(1-(RH/RH0))/(0.46*(h/h0)^(1/3));                %Eq 2.1-66
Fi0=FiRH*BETAfcm*BETAt0;                                %Eq 2.1-65
BETAH=150*(1+(1.2*RH/RH0)^18)*h/h0+250;                 %Eq 2.1-71

if BETAH>1500
   BETAH=1500;
End

BETAcdt=(((t(i)-t0)/t1)/(BETAH+((t(i)-t0)/t1)))^0.3;    %Eq 2.1-70
FI=Fi0*BETAcdt;                                         %Eq 2.1-64
Fi(i,:)=FI;

end
```

Appendix E

```
%%%%%%%%%%%%%%%%%%%%%%%%%%%%%%%%%%%%%%%%%%%%%%%%%%%%%%%%%%%%%%%%%%%%%%%%%%%%%%%
%
% Implementation of the material model describing creep in ABAQUS
%
%%%%%%%%%%%%%%%%%%%%%%%%%%%%%%%%%%%%%%%%%%%%%%%%%%%%%%%%%%%%%%%%%%%%%%%%%%%%%%%

*MATERIAL, NAME=SS0
*ELASTIC
41E9, 0.2
*DENSITY
      2.50E+03
*VISCOELASTIC, TIME=RELAXATION TEST DATA
*COMBINED TEST DATA
**    g_r(t)          ,     k_r(t)              ,     TIME
0.89596396885399  ,     0.89596396885399  ,     0.1
0.87492654725929  ,     0.87492654725929  ,     0.2
0.86099983761185  ,     0.86099983761185  ,     0.3
0.85034819206730  ,     0.85034819206730  ,     0.4
0.84163067929360  ,     0.84163067929360  ,     0.5
0.83420609984087  ,     0.83420609984087  ,     0.6
0.82771371938117  ,     0.82771371938117  ,     0.7
0.82192881447392  ,     0.82192881447392  ,     0.8
0.81670116831477  ,     0.81670116831477  ,     0.9
0.81192502452107  ,     0.81192502452107  ,     1
0.80752290254143  ,     0.80752290254143  ,     1.1
0.80343621536338  ,     0.80343621536338  ,     1.2
0.79961950909417  ,     0.79961950909417  ,     1.3
0.79603675892988  ,     0.79603675892988  ,     1.4
0.79265889500276  ,     0.79265889500276  ,     1.5
0.78946209613735  ,     0.78946209613735  ,     1.6
0.78642658076941  ,     0.78642658076941  ,     1.7
0.78353572986402  ,     0.78353572986402  ,     1.8
0.78077543755687  ,     0.78077543755687  ,     1.9
0.77813362169266  ,     0.77813362169266  ,     2
...
```

Appendix F

Swedish side

Segment	t_0	$f_{cm}(t_0)$	$f_{cm}(t_{eq})$
1.1	28	64,5	64,5
1.2	28	58,9	58,9
2	28	72,5	72,5
3	43	75,5	71,9
4	34	74,3	72,6
5	28	79,8	79,8
6	30	63,2	62,7
7	28	73,2	73,2
8	28	91,2	91,2
9	28	81,4	81,4
10	28	80,1	80,1
11	28	96,6	96,6
12	28	89,1	89,1
13	28	93,4	93,4
14	28	97,1	97,1
15	30	90,8	90,0
16	28	77,3	77,3
17	28	77,3	77,3
18	37	79,6	77,1
19	30	80,1	79,4
20	28	89,6	89,6
21	28	92,3	92,3
22	30	85,6	84,9
23	29	81,6	81,2
24	28	88,3	88,3
25	28	91,4	91,4

Norwegian side

Segment	t_0	$f_{cm}(t_0)$	$f_{cm}(t_{eq})$
1.1	33	68,7	67,4
1.2	28	79,1	79,1
2	28	65,3	65,3
3	30	68,4	67,8
4	28	62,7	62,7
5	28	69,9	69,9
6	28	81,5	81,5
7	28	81,7	81,7
8	28	70,5	70,5
9	31	83,4	82,4
10	28	91	91,0
11	30	97,1	96,3
12	28	90,5	90,5
13	28	92,2	92,2
14	34	88,8	86,8
15	28	80,5	80,5
16	27	82,9	83,3
17	38	87,7	84,6
18	28	82,4	82,4
19	28	93,1	93,1
20	28	92,2	92,2
21	28	84,3	84,3
22	30	81,5	80,8
23	30	88,2	87,5
24	28	83,3	83,3
25	28	90,6	90,6
26	131	95,1	83,1

t_0	Age of concrete at testing [days]
$f_{cm}(t_0)$	Compressive strength at t_0 [MPa]
t_{eq}	28 days
$f_{cm}(t_{eq})$	Equivalent compressive strength [MPa]at t_{eq} according to chapter 3

Appendix G

Swedish side

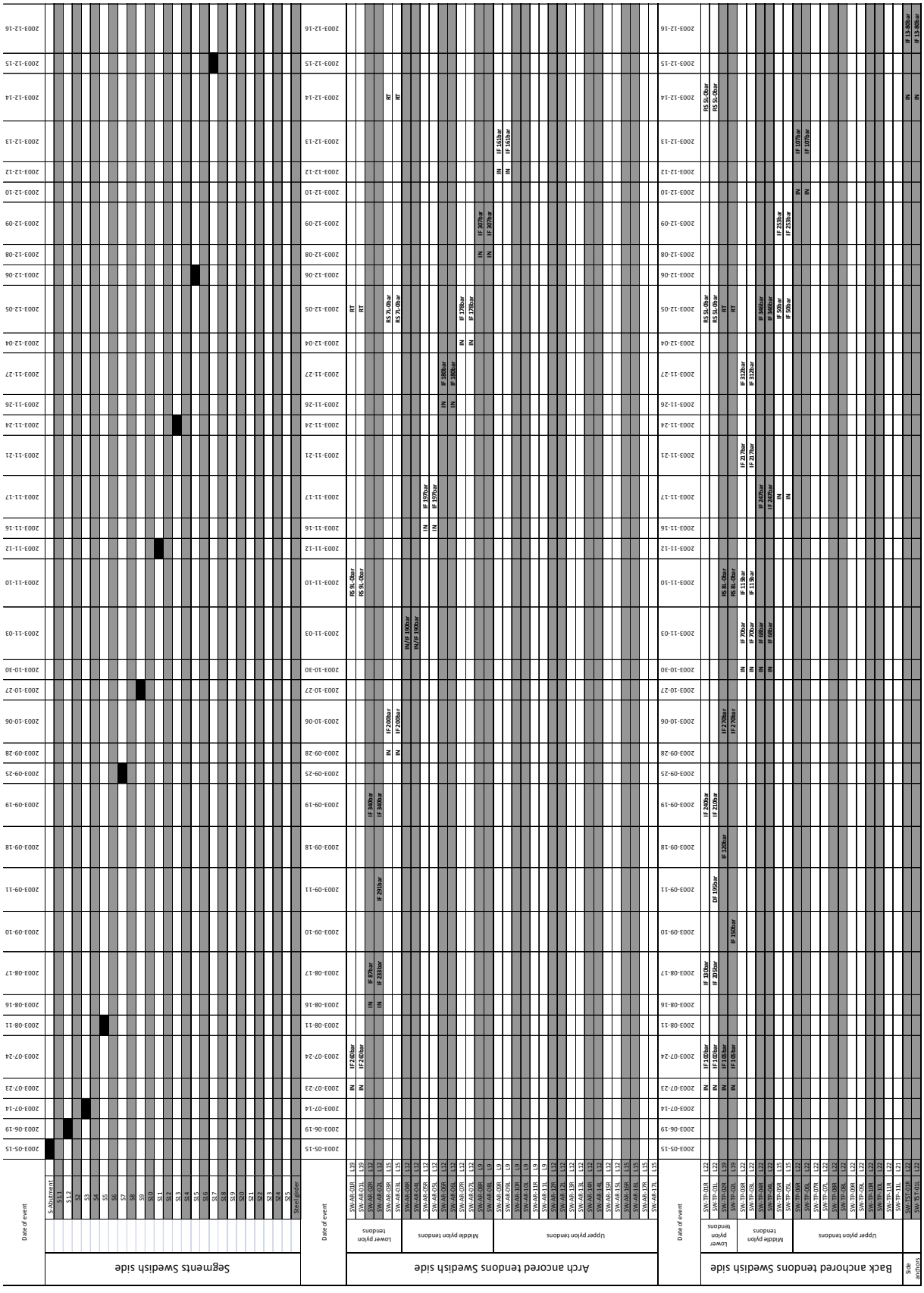

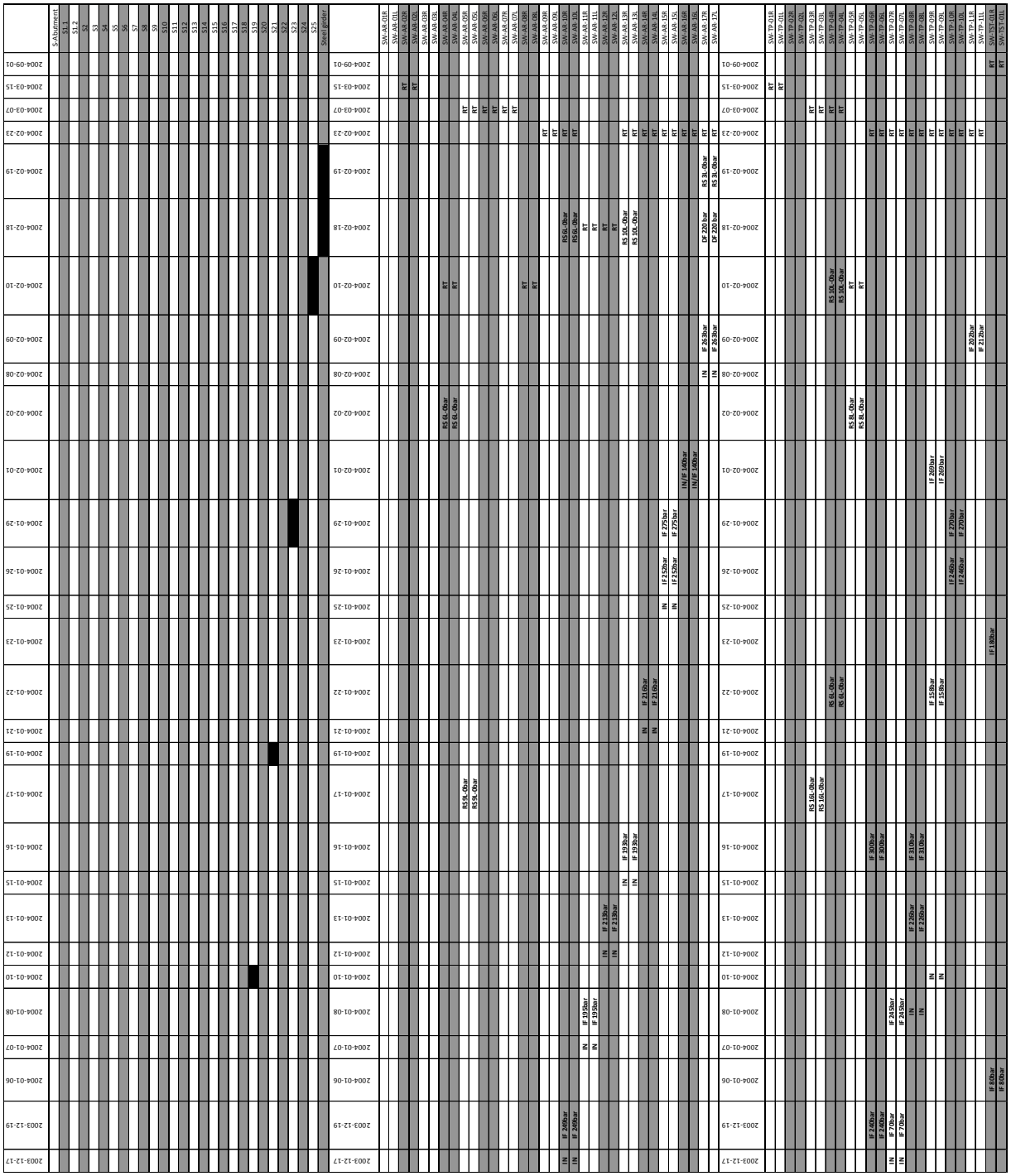

L Strands
IN Installation
IF Increase of force
RS Release of strands
RT Removal of tendon

Norwegian side

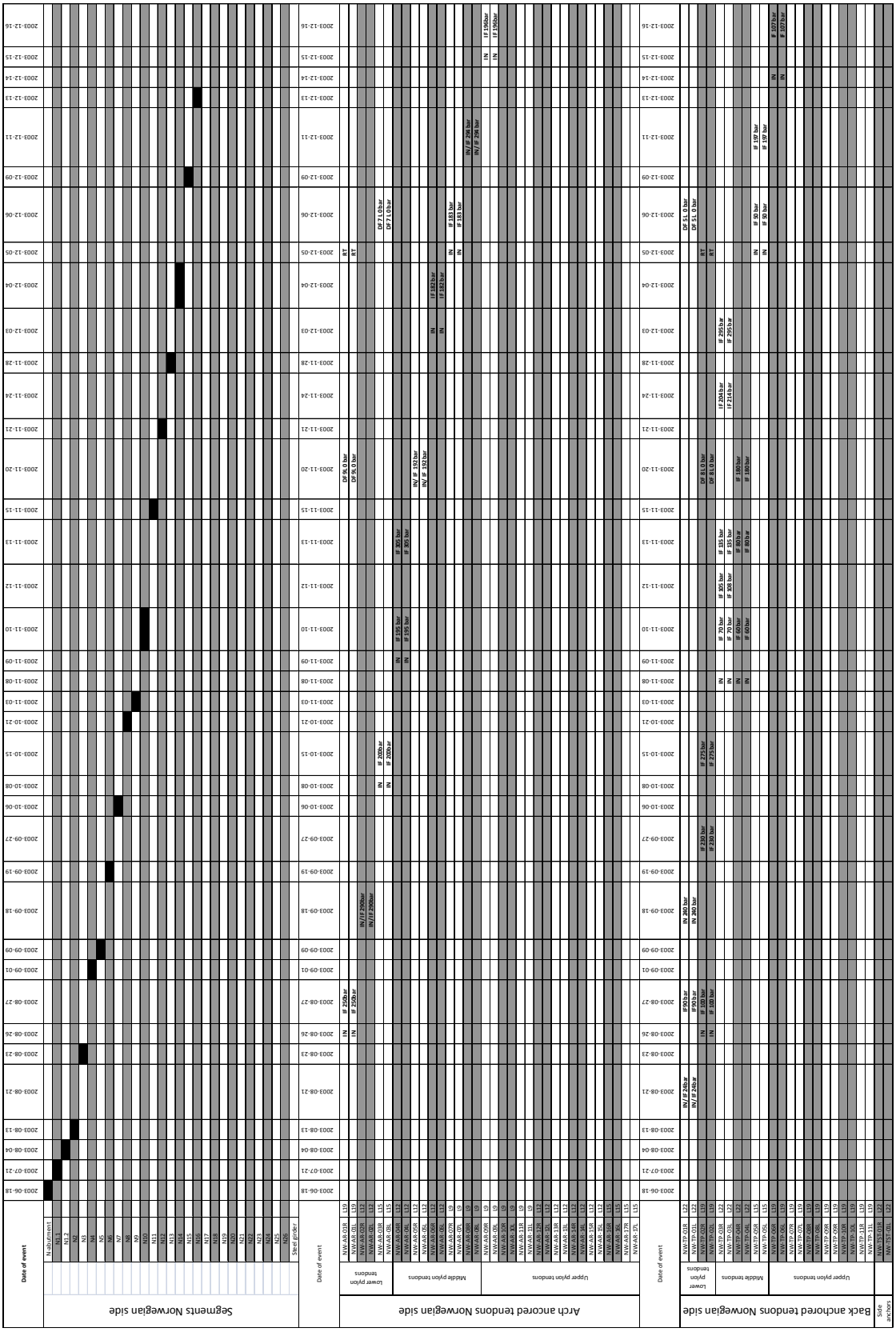

	2003-12-17	2003-12-18	2003-12-19	2004-01-04	2004-01-05	2004-01-06	2004-01-09	2004-01-13	2004-01-14	2004-01-15	2004-01-18	2004-01-19	2004-01-20	2004-01-22	2004-01-23	2004-01-24	2004-01-26	2004-01-28	2004-01-29	2004-01-31	2004-02-02	2004-02-04	2004-02-07	2004-02-10	2004-02-11	2004-02-12	2004-02-13	2004-02-15	2004-02-16	2004-02-17	2004-02-18	2004-02-19	2004-02-20	2004-02-22	2004-02-23	2004-03-07	2004-03-15	2004-09-01
N-abutment																																						
N1.1																																						
N1.2																																						
N2																																						
N3																																						
N4																																						
N5																																						
N6																																						
N7																																						
N8																																						
N9																																						
N10																																						
N11																																						
N12																																						
N13																																						
N14																																						
N15																																						
N16																																						
N17			■																																			
N18							■																															
N19										■																												
N20													■																									
N21																	■																					
N22																				■																		
N23																							■															
N24																										■												
N25																														■								
N26																																		■				
Steel girder																															■	■						

	2003-12-17	2003-12-18	2003-12-19	2004-01-04	2004-01-05	2004-01-06	2004-01-09	2004-01-13	2004-01-14	2004-01-15	2004-01-18	2004-01-19	2004-01-20	2004-01-22	2004-01-23	2004-01-24	2004-01-26	2004-01-28	2004-01-29	2004-01-31	2004-02-02	2004-02-04	2004-02-07	2004-02-10	2004-02-11	2004-02-12	2004-02-13	2004-02-15	2004-02-16	2004-02-17	2004-02-18	2004-02-19	2004-02-20	2004-02-22	2004-02-23	2004-03-07	2004-03-15	2004-09-01
NW-AR-01R																																						
NW-AR-01L																																						
NW-AR-02R																																					RT	
NW-AR-02L																																					RT	
NW-AR-03R	DF 0 bar																																					
NW-AR-03L	DF 0 bar																																					
NW-AR-04R																DF 6L 0bar																				RT		
NW-AR-04L																DF 6L 0bar																				RT		
NW-AR-05R																			DF 12L 0bar																	RT		
NW-AR-05L																			DF 12L 0bar																	RT		
NW-AR-06R																																				RT		
NW-AR-06L																																				RT		
NW-AR-07R																																				RT		
NW-AR-07L																																				RT		
NW-AR-08R																						RT																
NW-AR-08L																						RT																
NW-AR-09R																																			RT			
NW-AR-09L																																			RT			
NW-AR-10R					IN	IF 217 bar																							DF 6 L 0 bar						RT			
NW-AR-10L					IN	IF 217 bar																							DF 6 L 0 bar						RT			
NW-AR-11R								IN	IF 218 bar																RT													
NW-AR-11L								IN	IF 218 bar																RT													
NW-AR-12R											IN	IF 206 bar													RT													
NW-AR-12L											IN	IF 206 bar													RT													
NW-AR-13R														IN	IF 245 bar														DF 10 L 0 bar						RT			
NW-AR-13L														IN	IF 245 bar														DF 10 L 0 bar						RT			
NW-AR-14R																		IN	IF 221 bar																RT			
NW-AR-14L																		IN	IF 221 bar																RT			
NW-AR-15R																					IN	IF 258 bar													RT			
NW-AR-15L																					IN	IF 258 bar													RT			
NW-AR-16R																								IN	IF 130 bar										RT			
NW-AR-16L																								IN	IF 130 bar										RT			
NW-AR-17R																											IN	IF 262 bar			IF 8 L 310 bar, 7 L 300 bar	DF 1 L 0 bar	DF 2 L 0 bar		RT			
NW-AR-17L																											IN	IF 262 bar			IF 8 L 310 bar, 7 L 300 bar	DF 1 L 0 bar	DF 2 L 0 bar		RT			

	2003-12-17	2003-12-18	2003-12-19	2004-01-04	2004-01-05	2004-01-06	2004-01-09	2004-01-13	2004-01-14	2004-01-15	2004-01-18	2004-01-19	2004-01-20	2004-01-22	2004-01-23	2004-01-24	2004-01-26	2004-01-28	2004-01-29	2004-01-31	2004-02-02	2004-02-04	2004-02-07	2004-02-10	2004-02-11	2004-02-12	2004-02-13	2004-02-15	2004-02-16	2004-02-17	2004-02-18	2004-02-19	2004-02-20	2004-02-22	2004-02-23	2004-03-07	2004-03-15	2004-09-01
NW-TP-01R	DF 10L 0 bar																																				RT	
NW-TP-01L	DF 10 L 0 bar																																				RT	
NW-TP-02R																																						
NW-TP-02L																																						
NW-TP-03R																			DF 22 L 0 bar															IF 11 L 80 bar		RT		
NW-TP-03R																			DF 22 L 0 bar															IF 11 L 80 bar		RT		
NW-TP-04R																						DF 10 L 0 bar												DF 6L 80 bar		RT		
NW-TP-04L																						DF 10 L 0 bar												DF 6L 80 bar		RT		
NW-TP-05R																DF 8L 0 bar																				RT		
NW-TP-05L																DF 8L 0 bar																				RT		
NW-TP-06R						IF 206 bar									IF 250 bar																				RT			
NW-TP-06L						IF 206 bar									IF 250 bar																				RT			
NW-TP-07R				IN		IF 50 bar			IF 214 bar																										RT			
NW-TP-07L				IN		IF 50 bar			IF 214 bar																										RT			
NW-TP-08R												IN/IF 178 bar			IF 245 bar																				RT			
NW-TP-08L												IN/IF 178 bar			IF 245 bar																				RT			
NW-TP-09R																			IN/IF 158 bar																RT			
NW-TP-09R																			IN/IF 158 bar																RT			
NW-TP-10R																					IN	IF 228 bar													RT			
NW-TP-10L																					IN	IF 228 bar													RT			
NW-TP-11R																					IN								IF 227 bar						RT			
NW-TP-11L																					IN								IF 227 bar						RT			
NW-TST-01R		IN	IF 18 L 80 bar																																			RT
NW-TST-01L		IN	IF 18 L 80 bar																												12 L 180 bar							RT

Appendix H

Moments over the arch stage 1-6

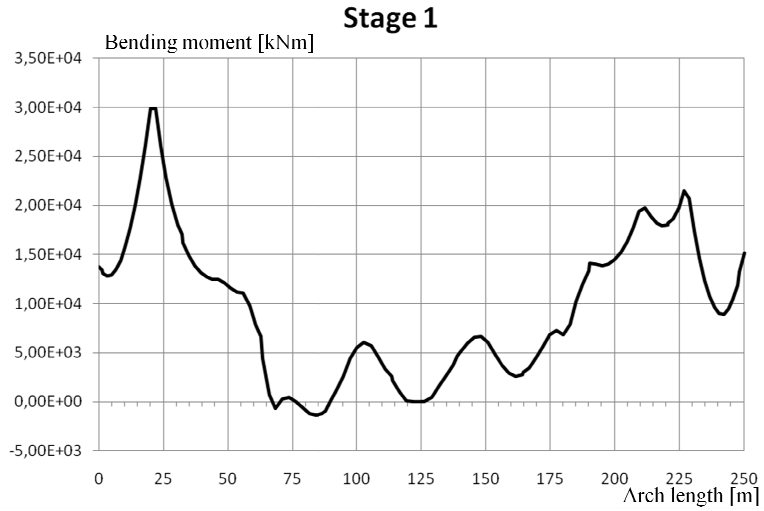

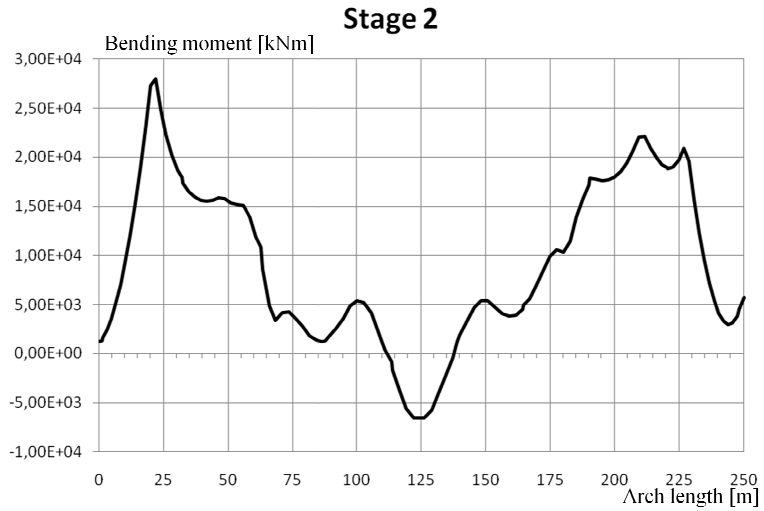

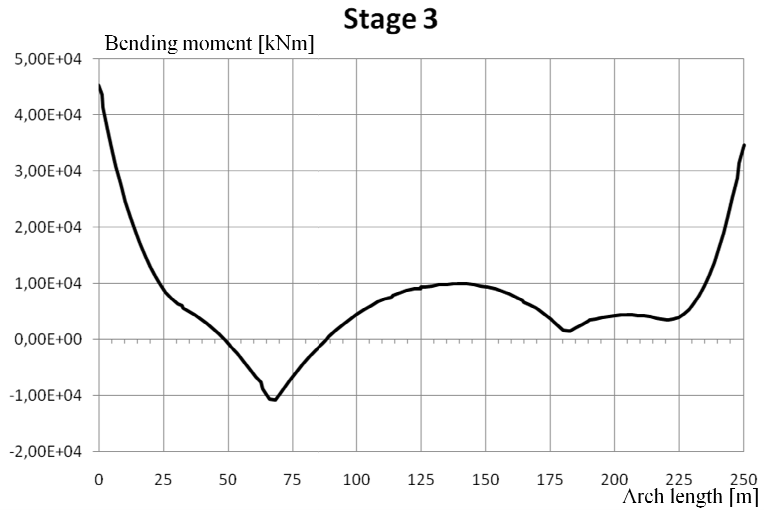

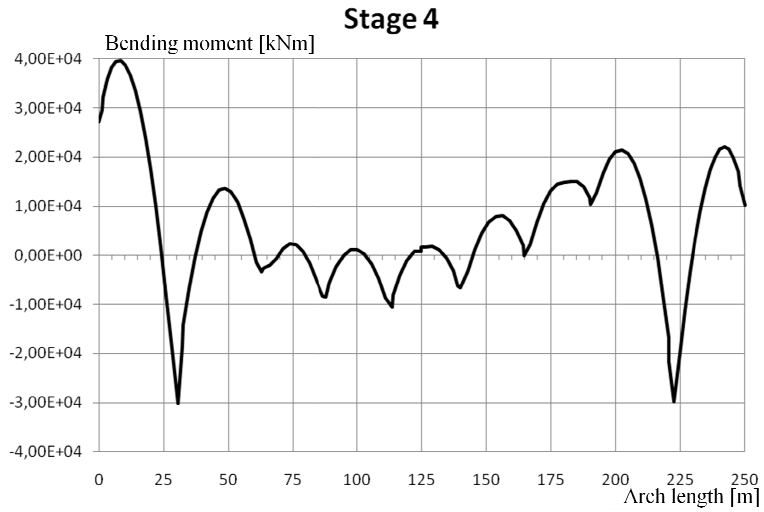
Stage 4
Bending moment [kNm]
4,00E+04
3,00E+04
2,00E+04
1,00E+04
0,00E+00
-1,00E+04
-2,00E+04
-3,00E+04
-4,00E+04
0
25
50
75
100
125
150
175
200
225
250
Arch length [m]

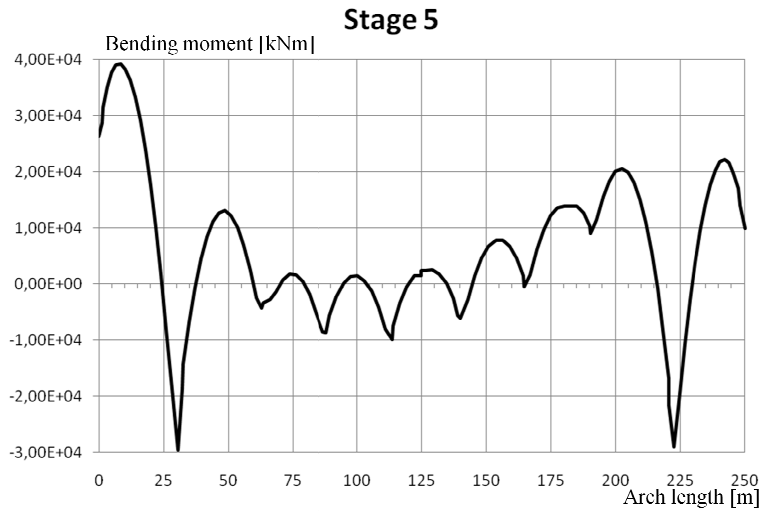
Stage 5
Bending moment [kNm]
4,00E+04
3,00E+04
2,00E+04
1,00E+04
0,00E+00
-1,00E+04
-2,00E+04
-3,00E+04
0
25
50
75
100
125
150
175
200
225
250
Arch length [m]

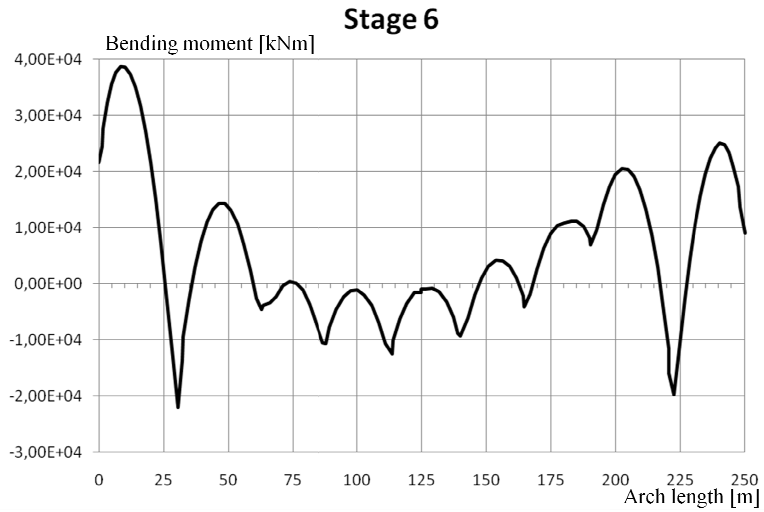
Stage 6
Bending moment [kNm]
4,00E+04
3,00E+04
2,00E+04
1,00E+04
0,00E+00
-1,00E+04
-2,00E+04
-3,00E+04
0
25
50
75
100
125
150
175
200
225
250
Arch length [m]

Normal forces over the Arch stage 1-6

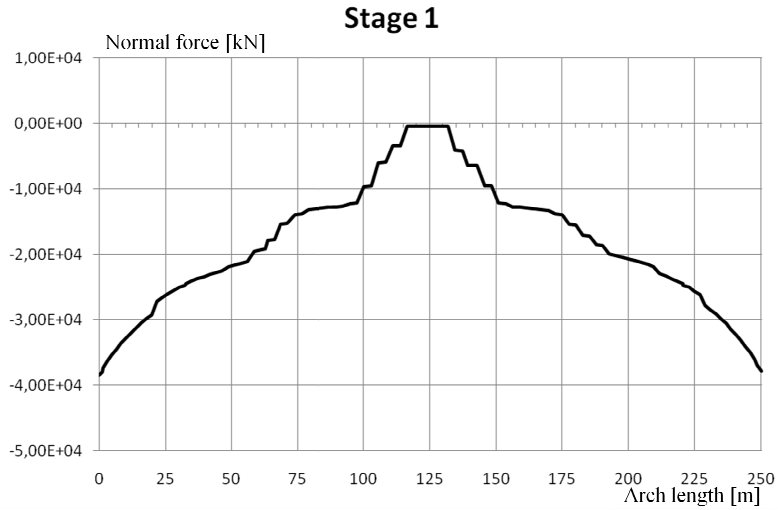

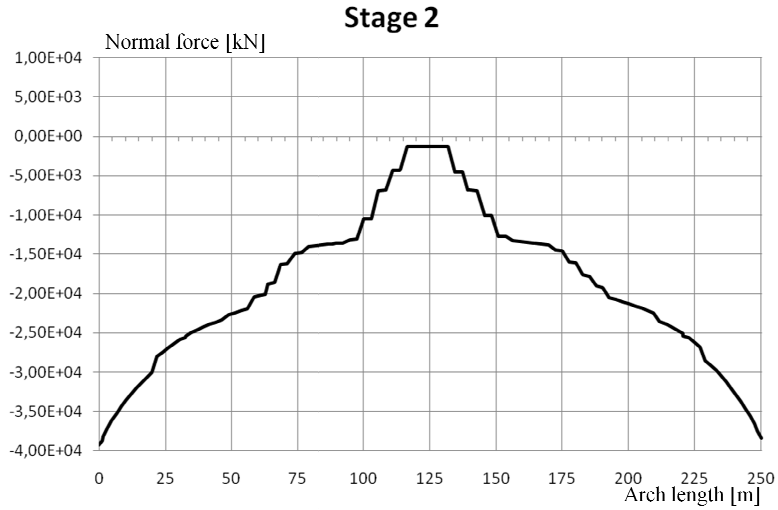

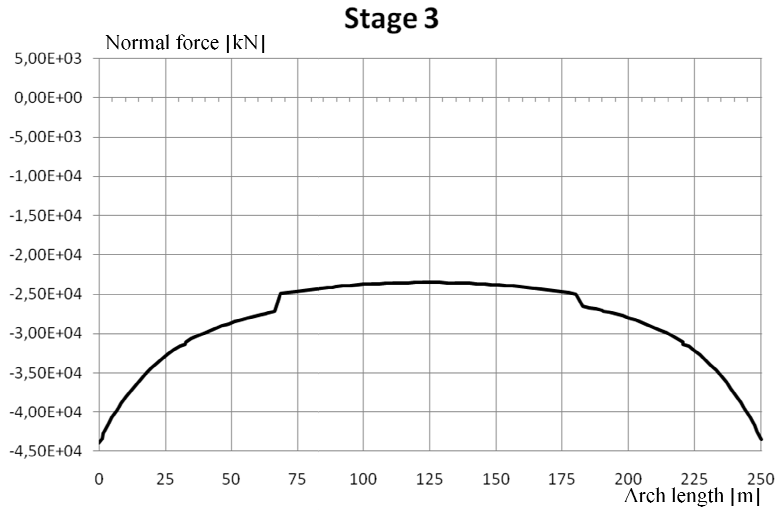

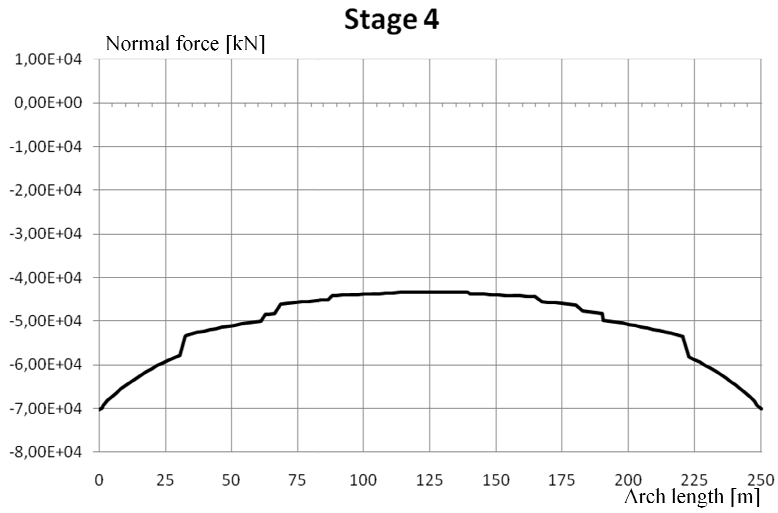
Stage 4
Normal force [kN]
1,00E+04
0,00E+00
-1,00E+04
-2,00E+04
-3,00E+04
-4,00E+04
-5,00E+04
-6,00E+04
-7,00E+04
-8,00E+04
0
25
50
75
100
125
150
175
200
225
250
Arch length [m]

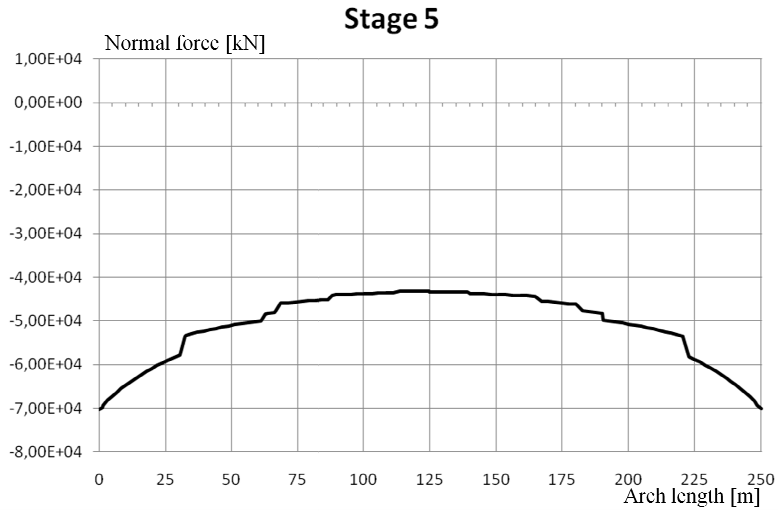
Stage 5
Normal force [kN]
1,00E+04
0,00E+00
-1,00E+04
-2,00E+04
-3,00E+04
-4,00E+04
-5,00E+04
-6,00E+04
-7,00E+04
-8,00E+04
0
25
50
75
100
125
150
175
200
225
250
Arch length [m]

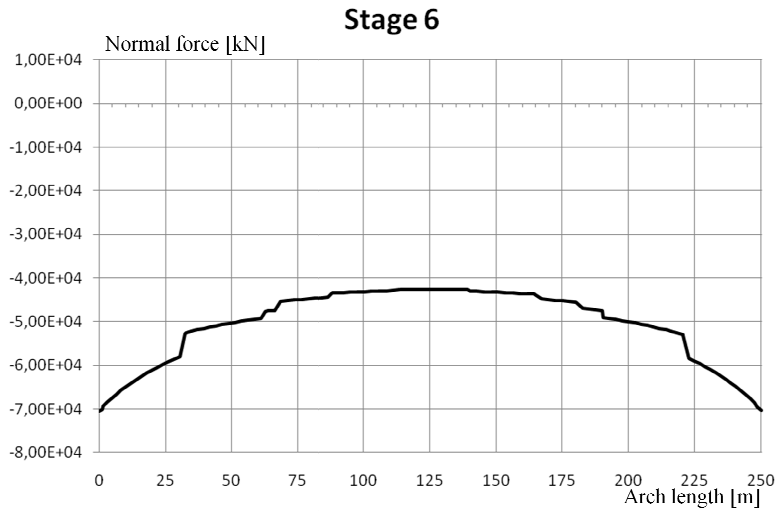
Stage 6
Normal force [kN]
1,00E+04
0,00E+00
-1,00E+04
-2,00E+04
-3,00E+04
-4,00E+04
-5,00E+04
-6,00E+04
-7,00E+04
-8,00E+04
0
25
50
75
100
125
150
175
200
225
250
Arch length [m]